# Correlation effects in vertical gated quantum dots

B. Szafran, S. Bednarek, and J. Adamowski*
*Faculty of Physics and Nuclear Techniques, University of Mining and Metallurgy (AGH), Kraków, Poland*
(Received 19 October 2002; revised manuscript received 20 December 2002; published 19 March 2003)

The influence of the electron-electron correlation on the electronic properties of vertical gated quantum dots with three-dimensional confinement has been studied by the configuration interaction method. We have found that the correlation is essential in the weakly confined electron systems and becomes negligibly small for the strongly confined electrons. We have determined the role of the correlation in the single-electron transport-spectroscopy experiments in the gated quantum dots. The correlation slightly changes the stability diagram, but considerably affects the magnetic-field dependence of the confined-electron energy spectra.

DOI: 10.1103/PhysRevB.67.115323 PACS number(s): 73.21.−b

The single-electron transport in the vertical gated quantum dot[1,2] (QD) has been described[3,4] with the use of the Hartree-Fock (HF) method. Although this method does not take into account the electron-electron correlation, good agreement has been obtained[3,4] with the stability diagram measured[2] without a magnetic field. However, the computational results[5] exhibit systematic deviations from the experimental data obtained in the magnetic field,[1] which can be ascribed to the electron-electron correlation. The configuration interaction (CI) method was applied[6–8] to the correlation in QD-confined electron systems in the framework of the two-dimensional parabolic confinement potential model. The parabolic potential was also used in calculations,[9,10] which account for the electron-electron correlation in the spin local density approximation. Matagne and Leburton[11] used the spin local density approach with the confinement potential derived from the Poisson equation. The results obtained[11] are rather far from the experimental data.[1,2] Based on the existing calculations,[6–11] one can hardly estimate the role of the correlation in the transport-spectroscopy experiments.[1,2] In the present paper, a systematic study of the correlation effects is performed for the vertical QD's by the CI method. We apply the model parabolic potential as well as the realistic confinement potential obtained from the self-consistent solution[4] of the Poisson-Schrödinger problem and discuss the role of the correlation in the single-electron transport via the vertical gated QD's.

We consider the three-dimensional system of $N$ electrons confined in the QD of the cylindrical symmetry. First, we solve the one-electron eigenproblem using trial wave functions of the form

$$\psi(\mathbf{r})=\sum_{k_x,k_y=0}^{k_x+k_y\leq k} c_{k_xk_y}x^{k_x}y^{k_y}\exp[-\alpha(x^2+y^2)-\beta z^2], \quad (1)$$

where $\alpha$ and $\beta$ are the nonlinear and $c_{k_xk_y}$ the linear variational parameters. Next, we use one-electron wave functions (1) to build the Slater determinants, which form the basis set for the diagonalization of the $N$-electron Hamiltonian by the CI method. The $N$-electron eigenstates possess definite $z$ components of the total angular momentum and the total spin; so they are labeled by the corresponding quantum numbers $(L,S)$. Basis (1), complemented by the spin wave function, allows for a construction of $\binom{(k+1)(k+2)}{N}$ Slater determinants with definite $L$ and $S$. For each $N$-electron state we use the basis composed of all Slater determinants with the required spin-orbital symmetry. The Gaussians in Eq. (1) lead to the analytical expressions for the Coulomb matrix elements. In the present paper, we consider the systems of two, three, and four electrons with $L=0,\ldots,6$.

The conditions of the single-electron tunneling[4] are determined by the chemical potentials, defined as $\mu_N=E_N-E_{N-1}$, where $E_N$ is the ground-state energy of the $N$-electron QD. In the vertical QD,[1] the confinement of electrons in the growth ($z$) direction is much stronger than the lateral confinement in the $x$-$y$ plane. Therefore, in the $N$-electron QD, all the confined electrons occupy the ground state of the quantized motion in the $z$ direction, which allows us to describe this state by a single $z$-dependent Gaussian [cf. Eq. (1)]. This leads to a slight overestimation of the ground-state energy, which is the same for all the occupied states; so it has no influence on the relative values of the chemical potentials of the electrons in the QD.

Before considering the real QD,[1,2] we study the correlation effects in the idealized QD described by the model confinement potential, which is assumed to be a rectangular potential well in the $z$ direction and a lateral potential $U_{conf}=m_e\omega^2(x^2+y^2)/2$, where $m_e$ is the electron effective band mass and $\hbar\omega$ is the confinement energy. We take the parameters of the nanostructure, which correspond to the cylindrical QD of Tarucha *et al.*[1]; e.g., the quantum well has width 12 nm in the $z$ direction and depth 220 meV. The values of all the other parameters are the same as in Ref. 4. In the gated QD,[1,2] the lateral confinement energy $\hbar\omega$ is not constant[4] but decreases from $\sim$6.7 to $\sim$5.4 meV when $N$ increases from 1 to 4. Therefore, in the present calculations with the model confinement potential, we take on $\hbar\omega=6$ meV. Moreover, we neglect the spin Zeeman effect.

In order to check the convergence of the present CI results, we have performed test calculations whose results are listed in Table I for $N=3$. In the further calculations, we adopt basis (1) with $k=5$. Based on the results of Table I, we estimate the precision for the energy levels considered to be about 0.1 meV. Therefore, throughout the present paper, we will call these CI results ''exact.'' Table I also shows that the accuracy of the HF method[12] is different for the different

 

TABLE I. Results of test calculations for the three-electron system confined in the lateral parabolic potential with $\hbar\omega=6$ meV and vertical double-barrier potential at $B=0$. $k$ determines the number of elements in one-electron basis (1). In the subsequent columns, we quote the energy (in meV) of the three lowest-energy states with quantum numbers $(L,S)$, given in the first row, calculated by the CI method with the numbers of Slater determinants given in parentheses. The results obtained by the HF method are listed in the last row. One-electron ground-state energy $E_1=-188.04$ meV. The top of the potential barrier is taken as the reference energy $(E=0)$.

| $k$ | (1,1/2) | (2,1/2) | (3,3/2) |
|---|---|---|---|
| 2 | −536.82 (15) | −533.33 (11) | −529.56 (2) |
| 3 | −538.20 (56) | −534.91 (49) | −530.66 (10) |
| 4 | −538.34 (161) | −535.19 (145) | −531.63 (38) |
| 5 | −538.40 (377) | −535.27 (354) | −531.66 (96) |
| 6 | −538.42 (785) | −535.29 (744) | −531.71 (218) |
| HF | −536.84 | −532.89 | −531.42 |

states. The difference between the exact and HF energy, i.e., the correlation energy, is considerably smaller for the spin-polarized state (3,3/2) than for the spin-unpolarized states (1,1/2) and (2,1/2). At zero magnetic field, the ground states of the systems with $N=2$, 3, and 4 electrons are labeled by (0,0), (1,1/2), and (0,1), respectively. For these states, using basis (1) with $k=5$, we have constructed 70, 377, and 2174 Slater determinants, respectively, and obtained the following total ground-state energies: $-367.94$ $(-366.84)$, $-538.42$ $(-536.84)$, and $-704.06$ $(-702.31)$ [in meV], where the HF estimate is given in the parentheses. These results show that the absolute errors of the HF total energy energy estimates increase with $N$. However, these errors partly cancel out when calculating the chemical potentials. The related differences of the chemical potentials calculated by the HF and CI methods are the following: $\Delta\mu_2=1.10$ meV, $\Delta\mu_3=0.48$ meV, and $\Delta\mu_4=0.17$ meV.

The magnetic-field evolution of the three-electron energy levels is displayed in Fig. 1, which shows that the correlation energy is nearly constant for each state considered, i.e., independent of the magnetic field. We note that the HF method can fail in predicting the ground state of the system. For the three-electron system the ground state changes with the magnetic field as follows: this is state (1,1/2) for $B<4.6$ T, state (2,1/2) for $4.6\ \mathrm{T}\leqslant B\leqslant 5.7$ T, and state (3,3/2) for $B>5.7$ T. However, according to the HF approach, state (1,1/2) would possess the lowest energy for $B<3.8$ T, while for the higher magnetic field state (3,3/2) would become the ground state. As a result, the HF method underestimates the magnetic field, which induces the spin polarization, and does not predict state (2,1/2) to be the ground state.

The chemical potentials calculated by the CI and HF methods are displayed in Figs. 2(a)–2(c) for different confinement strengths. In the case of weak confinement [Fig. 2(a)], the HF results become unreliable both quantitatively and qualitatively. In particular, the HF method predicts the incorrect symmetry of the ground state. For example, the low-spin state (2,0), which is the ground state of the four-

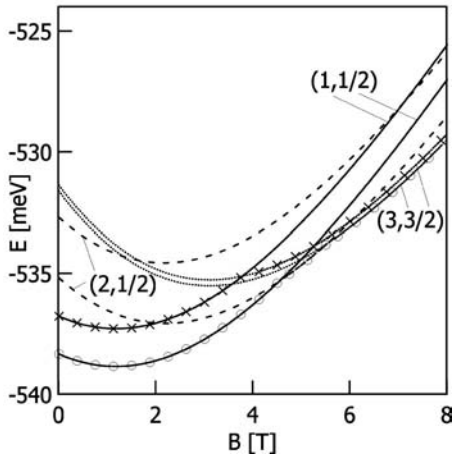


FIG. 1. Energy $E$ of the three-electron system in the vertical QD with the parabolic lateral confinement ($\hbar\omega=6$ meV) as a function of magnetic field $B$. Solid lines correspond to state (1,1/2), dashed lines to state (2,1/2), and dotted lines to state (3,3/2). For each pair of the curves the lower (upper) one shows the CI (HF) results. The ground-state energy determined by the CI (HF) method is marked by circles (crosses).

electron system in a wide range of the magnetic field, is erroneously predicted to be the excited state in the HF method. QD's with the weak confinement were fabricated by Ashoori *et al.*[13] However, the experimental spectra for these dots are affected by random local fluctuations of the confinement potential. Therefore, the parabolic model potential seems to be oversimplified for these QD's.

Figure 2(b) shows the results for the intermediate confinement. With one exception, the increasing magnetic field leads to the increase of the total spin in the ground-state transformations. Since the HF method works better for the spin-polarized states, the critical values of the magnetic field for these transformations are underestimated. In the four-electron system, the transition $(0,1)\rightarrow(2,0)$ at $B=0.5$ T is the only one in which the total spin decreases and the corresponding critical magnetic field is overestimated by the HF method, which prefers the spin polarization. We note that the intermediate confinement corresponds to the QD of Tarucha *et al.*[1] In this case, the HF results are in qualitative agreement with the exact results. The only exception is the omittance of the (2,1/2) ground state in the three-electron system [Fig. 2(b)]. However, the cusp corresponding to the $(1,1/2)\rightarrow(2,1/2)$ transition is rather smooth. Therefore, this transition is hardly visible in the experimental data.[1]

The results for the strong confinement are displayed in Fig. 2(c), which shows that the agreement between the HF and CI results is better than in the case of the intermediate confinement. In the strongly confined electron systems, the multiconfiguration basis reduces to one dominating configuration; i.e., the correlation is small. The results of Fig. 2(c) indicate that the HF method can be used as a computational tool of sufficiently high precision for the QD's with the strong confinement potential, e.g., for the self-assembled quantum dots, in which $\hbar\omega>10$ meV.[14]

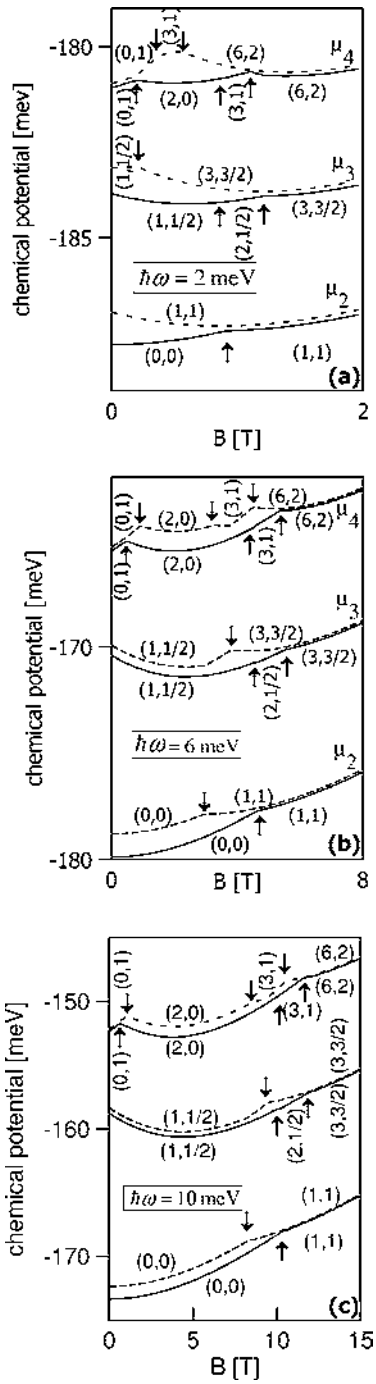


FIG. 2. Chemical potentials $\mu_N$ of $N=2$, 3, 4 electrons confined in the vertical QD with the confinement energy (a) $\hbar\omega=2$ meV, (b) $\hbar\omega=6$ meV, and (c) $\hbar\omega=10$ meV, as functions of magnetic field *B*. The results obtained by the CI (HF) method are displayed by solid (dashed) lines. Quantum numbers $(L,S)$ correspond to the ground state. The magnetic-field-induced ground-state transformations calculated by the CI (HF) method are shown by the arrows up (down).

The exact chemical potentials exhibit the same qualitative magnetic-field dependence for the confinement potentials studied [cf. Figs. 2(a)–2(c)]. In all the cases studied in this paper, the magnetic-field induces the ground-state transformations in the same order independently of the strength of the confinement. In the high-magnetic field regime, states (1,1), (3,3/2), and (6,2) of the two-, three-, and four-electron systems, respectively, correspond to a maximum density droplet (MDD).[15] We note that—for these states—the HF method yields very accurate results. At the higher magnetic fields than those considered in the present paper, the MDD becomes unstable against a formation of a Wigner molecule.[16–19] Based on the high accuracy of the HF method for the high-field spin-polarized states, we expect that the unrestricted HF method with a properly chosen basis[19] will yield reliable results for the Wigner molecules. For the MDD, the unrestricted and restricted HF methods yield the same results. In this state, the electron charge density obtained by both the HF methods reproduces the symmetry of the confinement potential. However, only the unrestricted HF method accounts for the breakdown of the MDD and the formation of the Wigner molecule.[17–19] In this way, the unrestricted HF method can provide at least some collective effects in the confined electron system. Therefore, the results of the restricted HF approach are more suitable as the reference data in the discussion of the correlation effects.[20]

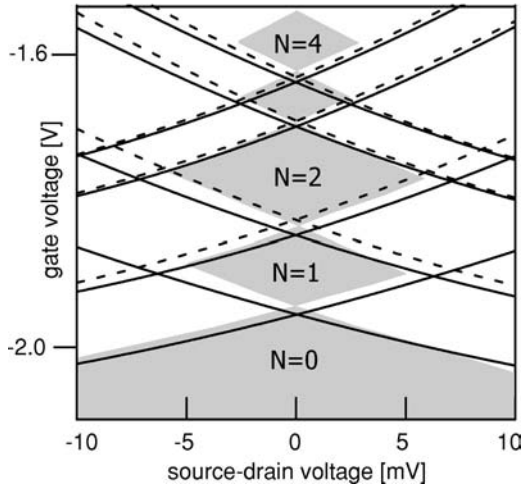


FIG. 3. Stability diagram with Coulomb diamonds. The experimental data (Ref. 2) are depicted by the shaded areas. Solid (dashed) curves show the boundaries of the Coulomb diamonds calculated by the CI (HF) method.

Now, we consider the effect of correlation on the single-electron transport in the real QD.[1,2] For this purpose, we have introduced the CI method into the self-consistent procedure, elaborated in our previous work,[4] in order to solve the Poisson-Schrödinger problem for the vertical gated QD.[1,2] We are still using the HF method[21] to determine the confined charge density in the self-consistency loop[4] for the electrostatics of the nanodevice, since the charges outside the QD perceive the averaged confined electron charge only. The CI method is applied to the evaluation of the energy of the *N*-electron system confined in the QD, which allows us to increase the accuracy of the energy calculations. The results are displayed in Fig. 3, which shows the stability diagram with the Coulomb diamonds measured by Kouwenhoven *et al.*[2] and their borders calculated by the CI and HF methods. We note that the both the methods lead to similar results.

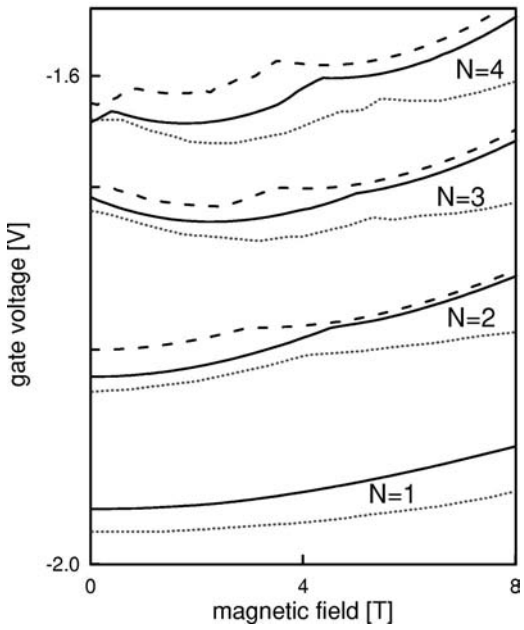


FIG. 4. Gate voltage corresponding to the current peaks as a function of the magnetic field. Dotted, solid, and dashed lines correspond to the experimental (Ref. 2), CI, and HF results, respectively.

The significant differences that occur for the upper boundaries of the first diamond and the lower boundaries of the second diamond are due to the fact that the largest difference between the HF and CI chemical potentials appears for $N=2$. It is just chemical potential $\mu_2$ that determines these boundaries.[4]

The magnetic-field dependence of the gate voltage, at which the single-electron tunneling occurs, is plotted in Fig. 4. The cusps on the curves (Fig. 4) correspond to the magnetic-field-induced ground-state transformations in the $N$-electron QD. We see that the CI results are considerably closer to the experimental data than the HF results and the HF method underestimates the critical magnetic fields for the ground-state transformations. This means that the electron-electron correlation plays an important role in the single-electron transport in the external magnetic field. For $N=1$ there is no correlation; therefore, the discrepancy between the measured and calculated plots (cf. Fig. 4, $N=1$) illustrates the precision of the present modeling of the vertical QD. The difference in the slopes of these plots, which is visible in Fig. 4, indicates that the confinement potential in the real nanostructure is slightly stronger than that used in our modeling.

The conditions of the single-electron transport via the gated QD (Refs. 1 and 2) are determined by the QD chemical potential,[4] which is calculated as the ground-state energy difference. If the ground-state energies are determined with a comparable accuracy, the errors cancel out and the chemical potential can be evaluated with a sufficient precision. This explains why the HF approach[4] leads to a good agreement with experiment[2] for the Coulomb diamonds (cf. Fig. 3). The critical magnetic fields for the ground-state transformations are directly determined by the ground-state energy. The HF method works with the different accuracy for the different states (cf. Fig. 1). Therefore, the magnetic field, which induces the ground-state transformations, i.e., changes the order of the energy levels associated with the states of the different spin-orbital symmetry, can be inaccurately estimated by the HF method.

In summary, we have shown that the correlation considerably changes the energy of the weakly confined electron systems. In the single-electron transport through the vertical gated QD's, the correlation slightly modifies the boundaries of the Coulomb diamonds in the stability diagram, but considerably affects the QD energy spectra in the external magnetic field.

This work has been partly supported by the Polish Government Scientific Research Committee (KBN) under Grant No. 5P03B 4920. B.S. acknowledges the support of the Foundation for Polish Science (FNP).

*Electronic address: adamowski@ftj.agh.edu.pl

[1] S. Tarucha, D.G. Austing, T. Honda, R.J. van der Hage, and L.P. Kouwenhoven, Phys. Rev. Lett. **77**, 3613 (1996).
[2] L.P. Kouwenhoven, T.H. Oosterkamp, M.W.S. Danoesastro, M. Eto, D.G. Austing, T. Honda, and S. Tarucha, Science **278**, 1788 (1997).
[3] S. Bednarek, B. Szafran, and J. Adamowski, Phys. Rev. B **61**, 4461 (2000).
[4] S. Bednarek, B. Szafran, and J. Adamowski, Phys. Rev. B **64**, 195303 (2001).
[5] B. Szafran, S. Bednarek, and J. Adamowski, Phys. Rev. B **65**, 035316 (2002).
[6] M. Eto, Jpn. J. Appl. Phys., Part 1 **36**, 3924 (1997).
[7] D. Pfannkuche, V. Gudmundsson, and P.A. Maksym, Phys. Rev. B **47**, 2244 (1993).
[8] S.A. Mikhailov and N.A. Savostianova, Phys. Rev. B **66**, 033307 (2002).
[9] S.M. Reimann, M. Koskinen, M. Manninen, and B.R. Mottelson, Phys. Rev. Lett. **83**, 3270 (1999).
[10] O. Steffens, M. Suhrke, and U. Rössler, Physica B **256-258**, 147 (1998).
[11] P. Matagne and J.-P. Leburton, Phys. Rev. B **65**, 235323 (2002).
[12] In the calculations with the model confinement potential, we require the HF one-electron wave functions to be the eigenfunctions of the $z$ component of the angular momentum.
[13] R.C. Ashoori, N.B. Zhitenev, L.N. Pfeiffer, and K.W. West, Physica E (Amsterdam) **3**, 15 (1998).
[14] B.T. Miller *et al.*, Phys. Rev. B **56**, 6764 (1997).
[15] A.H. McDonald, S.R.E. Yang, and M.D. Johnson, Austral. J. Phys. **46**, 345 (1993).
[16] K. Jauregui, W. Häusler, and B. Kramer, Europhys. Lett. **24**, 581 (1993); P.A. Maksym *et al.*, J. Phys.: Condens. Matter **12**, R299 (2000).
[17] H-M. Müller and S.E. Koonin, Phys. Rev. B **54**, 14 532 (1996).
[18] C. Yannoulenas and U. Landman, Phys. Rev. Lett. **82**, 5325 (1999).

[19] B. Szafran, S. Bednarek, and J. Adamowski, Phys. Rev. B **67**, 045311 (2003).

[20] P. Knowles, M. Schültz, and H.-J. Werner, in *Modern Methods and Algorithms of Quantum Chemistry*, edited by J. Grotendorst, NIC Series, Vol. 3 (John von Neumann Institute of Computing, Jülich, 2000), p. 97.

[21] The HF results for the real QD taken from Refs. 4 and 5 have been obtained by the unrestricted HF method.

# Magnetic-field-induced transformations of Wigner molecule symmetry in quantum dots

B. Szafran, S. Bednarek, and J. Adamowski
*Faculty of Physics and Nuclear Techniques, University of Mining and Metallurgy (AGH), Kraków, Poland*
(Received 5 November 2002; published 15 January 2003)

A theoretical study has been performed for the ground-state spatial configuration of Wigner molecules with $N=2,\ldots,20$ electrons in quantum dots subjected to an external magnetic field. We have shown that—for $N\geqslant 6$—the Wigner molecule formed in the magnetic field above the maximum-density-droplet instability has a different shape than in the high-field limit. We have found several magnetic-field-induced transitions between molecular phases with different spatial symmetry.

DOI: 10.1103/PhysRevB.67.045311 PACS number(s): 73.21.−b, 73.22.Gk

A quantum dot (QD), a semiconductor nanostructure that confines electrons in three dimensions, can be used as a unique physical laboratory for studying properties of electron systems. In particular, the QD-confined electron systems (artificial atoms) are much more sensitive to the external magnetic field than the natural atoms.[1,2]

The charge distribution in the artificial atom is a result of an interplay between the electron-electron Coulomb interaction and the one-electron effects. If the Coulomb energy is small compared to the one-electron energy-level separation, the occupied spin orbitals are only slightly perturbed by the interaction and the electron distribution reproduces the symmetry of the external potential. If, however, the one-electron energy levels are nearly degenerate, the occupied states are superpositions of a large number of noninteracting electron spin orbitals. In this case, the electrons exhibit a pronounced tendency to be localized at different space sites. Therefore the electron distribution can lose the symmetry of the confining potential and take a form of a set of separate islands. This distribution resembles that of a classical charge-carrier system[3] and is called a Wigner crystal[4] (in the systems with translational symmetry) or a Wigner molecule[5,6] (in the QD's). The Wigner molecules can be formed in large structures,[7–9] for which the quantum size effects disappear. They can also be created in nanostructures by a strong external magnetic field.[10–15]

The application of the external magnetic field leads to relative shifts of the energy levels corresponding to different spin-orbital configurations.[2,16] In consequence, the ground-state configuration changes when the magnetic field increases. At a certain, sufficiently high, magnetic field all the electrons have parallel spins and occupy orbitals with successive magnetic quantum numbers.[13] In this state, called a maximum density droplet[17] (MDD), the electron charge distribution still possesses the symmetry of the confinement potential. If, however, the magnetic field increases further, all the occupied energy levels approach the lowest Landau level and become degenerate. Then, the Coulomb interaction leads to a rapid change of the electron distribution. As a result, the confinement-potential symmetry of the electron density is broken and the Wigner molecule is formed. The breakdown of the MDD (Refs. 18 and 19) has recently been observed[20] in the vertical gated QD.[1]

In the present paper, we consider the shape of the Wigner molecule ground state as a function of the magnetic field above the MDD regime. For this purpose, we apply a theoretical approach designed for a description of Wigner molecules in QD's at high magnetic fields. Let us first consider a single electron in a magnetic field, which is so high that the confinement potential can be neglected in the first approximation. We assume the magnetic field to be perpendicular to the QD region ($x$-$y$ plane), i.e., $\mathbf{B}=(0,0,B)$, and apply the Landau (nonsymmetric) gauge for the vector potential, i.e., $\mathbf{A}=(-By,0,0)$. The one-electron Hamiltonian has the form

$$h=-\frac{\hbar^2}{2m}\left(\frac{\partial^2}{\partial x^2}+\frac{\partial^2}{\partial y^2}+2i\alpha y\frac{\partial}{\partial x}-\alpha^2y^2\right), \qquad (1)$$

where $m$ is the electron effective mass, $\alpha=eB/\hbar=m\omega_c/\hbar$, and $\omega_c=eB/m$ is the cyclotron frequency. The ground-state energy of Eq. (1) is equal to $E_0=\hbar\omega_c/2$, i.e., the energy of the lowest Landau level, which is infinitely-fold degenerate. Due to this degeneracy the ground-state eigenfunction of Eq. (1) can be chosen in many forms. We choose the following one:

$$\Psi_{\mathbf{R}}(x,y)=(\alpha/2\pi)^{1/2}\exp\{-(\alpha/4)[(x-X)^2+(y-Y)^2] -(i\alpha/2)(x-X)(y+Y)\}, \qquad (2)$$

which—for arbitrary $\mathbf{R}=(X,Y)$—fulfills the eigenequation of Eq. (1) for eigenvalue $E_0$. We note that the charge distribution generated by wave function (2) is the Gaussian centered at point $\mathbf{R}$, which can be treated as the center of the Landau orbit. The wave functions of form (2) are convenient for a construction of a multicenter variational basis, which is appropriate for a description of the Wigner molecules. A similar approach, but in the symmetric gauge, has been applied to the Wigner crystals.[4]

Now, we consider the system of $N$ electrons confined in the two-dimensional harmonic-oscillator potential and subjected to the external magnetic field. This system is described by the Hamiltonian

$$H=\sum_{i=1}^{N}\left(h_i+\frac{1}{2}m\omega_0^2r_i^2+\sum_{j<i}^{N}\frac{\kappa e^2}{\varepsilon r_{ij}}\right)-\frac{1}{2}Ng^*\mu_BB, \qquad (3)$$

where $h_i$ is Hamiltonian (1) for the $i$th electron, $\mathbf{r}_i=(x_i,y_i)$, $r_{ij}=|\mathbf{r}_i-\mathbf{r}_j|$, $\kappa=1/4\pi\varepsilon_0$, $\varepsilon$ is the dielectric constant, $g^*$ is the effective Lande factor, and $\mu_B$ is the Bohr magneton. The last term in Hamiltonian (3) is the Zeeman

 

TABLE I. Ground-state energy of $N$-electron Wigner molecule for $B=20$ T. In the second (third) line the results of Ref. 10 (present paper) are listed. Energy is expressed in meV.

| $N$ | 1 | 2 | 3 | 4 | 6 | 10 | 20 |
|---|---|---|---|---|---|---|---|
| Ref. 10 | 17.25 | 40.09 | 66.44 | 96.46 | 166.35 | 339.93 | 937.97 |
| Present | 17.25 | 40.15 | 66.45 | 96.42 | 166.27 | 339.69 | 936.56 |

energy of $N$ spin-polarized electrons. We apply the material parameters of GaAs, for which we take on the same values as in Ref. 10, i.e., $m=0.067m_e$, $\varepsilon=12.9$, $g^*=0.54$, and $\hbar\omega_0=3$ meV.

The $N$-electron problem has been solved by the unrestricted Hartree-Fock method with the one-electron wave functions expanded in multicenter basis (2),

$$\Phi(x,y)=\sum_{i=1}^{N} c_i \Psi_{\mathbf{R}_i}(x,y), \tag{4}$$

where $c_i$ are the linear variational parameters and the basis functions $\Psi_{\mathbf{R}_i}(x,y)$ are taken on in form (2) with parameter $\alpha$ replaced by a nonlinear variational parameter $\alpha^*$. In the wave function (4), the positions $\mathbf{R}_i=(X_i,Y_i)$ of $N$ centers are found from the equilibrium positions $\mathbf{R}_i^c$ of the classical counterpart of the considered $N$-electron system as follows: $\mathbf{R}_i=\sigma\mathbf{R}_i^c$, where the scaling factor $\sigma$ is treated as the second nonlinear variational parameter. It appears that $\alpha^*>\alpha$, since the QD confinement potential enhances the localization of electrons. If the exchange interaction does not vanish, the interelectron repulsion is weakened and the average electron-electron distances are diminished, i.e., $\sigma<1$.

In the parabolic confinement, the classical, equally charged, particles take on the shell-like equilibrium configurations.[3] This feature is qualitatively reproduced in the Wigner molecules. Therefore we label the spatial configurations of the Wigner molecules by the numbers of electrons in the subsequent shells, e.g., $N_1$-$N_2$-$N_3$ denote the state, in which $N_1$, $N_2$, and $N_3$ electrons occupy the inner, middle, and outer shell, respectively.

The present calculations have been performed for $N=1,\ldots,20$ electrons. The results of test calculations with basis (4) are listed in Table I and compared with those of Miller and Koonin,[10] who applied the symmetric gauge and the unrestricted Hartree-Fock method with the basis functions of the definite angular momentum. Table I shows that the present variational estimates are very close to those of Ref. 10 for $N=1,\ldots,3$ and become better for $N\geqslant 4$. We note that the present approach, in which only one basis function is associated with each electron, requires a considerably smaller numerical effort than that of Ref. 10, in which a superposition of a very large number of angular momentum eigenstates is needed to describe the islandlike charge distribution.

Figure 1 shows the ground-state energy of the six-electron system calculated with multicenter basis (4) generated from the scaled classical configurations 0-6 in which the electrons form a hexagon, and 1-5 with one of the electrons localized at the origin and five others forming a pentagon around it.

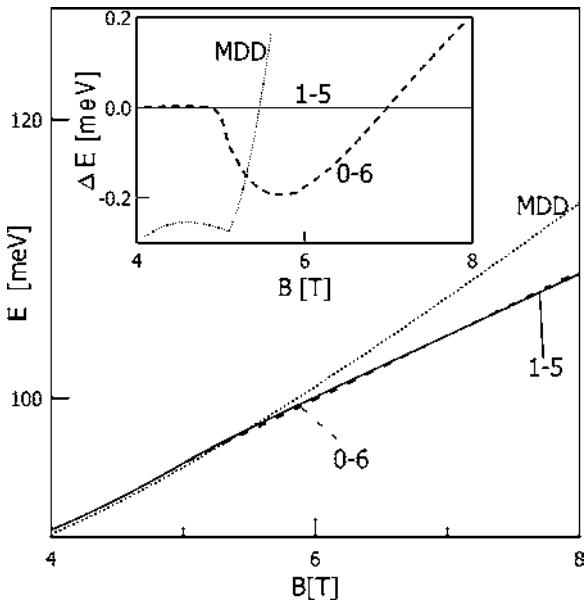


FIG. 1. Ground-state energy $E$ of the six-electron Wigner molecule with shell-structure 1-5 (solid line) and 0-6 (dashed line), and the MDD phase (dotted line) as a function of magnetic field $B$. Inset shows the energy $\Delta E$ of the 0-6 Wigner molecule and MDD determined with respect to the energy of the 1-5 (high-field) phase.

The dotted line shows the results of our additional calculations for the cylindrically symmetric MDD state obtained in the symmetric gauge by the Hartree-Fock method with finite difference approach, free of a possible variational overestimation of the MDD energy. The inset of Fig. 1 shows that the energy calculated with respect to that of the 1-5 configuration exhibits characteristic cusps near $B=5.3$ T. For $B<5.3$ T the MDD state possesses the lowest energy. In the MDD-stability regime, the energy obtained with the multicenter basis for both the 0-6 and 1-5 configurations follow the MDD energy quite well. Figure 2 displays the charge-density distribution for the three configurations of the six-electron system. It is remarkable that the charge density obtained with the 1-5 multicenter basis [cf. Fig. 2(a)] well approximates the MDD charge-density distribution. The slight deviations from the circular symmetry are responsible for the overestimation of the MDD ground-state energy. If the magnetic field increases above 5.3 T, the electron system becomes the Wigner molecule with the 0-6 shell structure [cf. Fig. 2(b)]. If the magnetic field exceeds 7 T, the Wigner

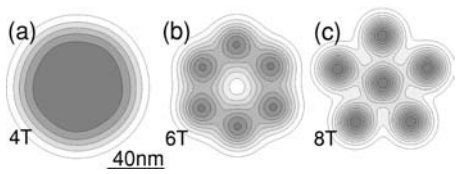


FIG. 2. Electron density distribution for six electrons in (a) approximation of the MDD phase for $B=4$ T calculated with the six-center wave function in 1-5 configuration and the Wigner molecules with shell structures (b) 0-6 for $B=6$ T and (c) 1-5 for $B=8$ T. The darker the shade of grey the larger electron density. The bar shows the length scale.

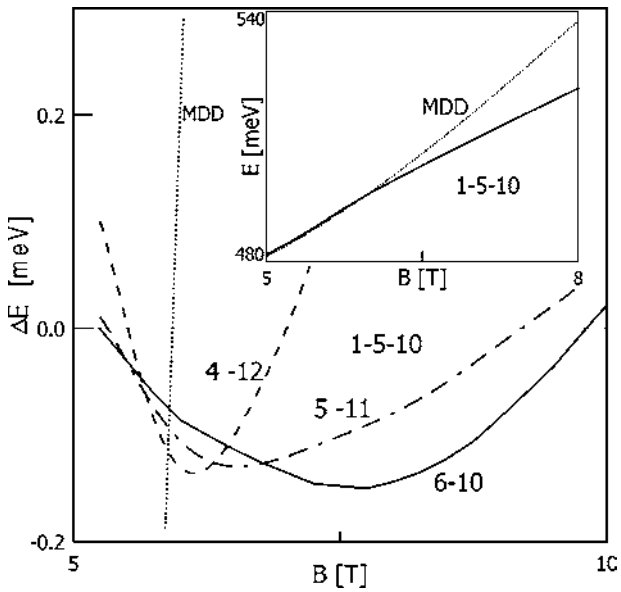


FIG. 3. Energy separation $\Delta E$ from the ground-state energy of the 1-5-10 Wigner molecule to those of the 6-10 (solid line), 5-11 (dash-dotted), and 4-12 (dashed) phases. The corresponding results for the 16-electron MDD are plotted by the dotted line. Inset displays the ground-state energy of the 1-5-10 Wigner molecule and MDD.

molecule changes its shape into the 1-5 configuration [cf. Fig. 2(c)], which is the lowest-energy configuration of the system of six classical charge carriers. The present results show that the six-electron Wigner molecule created after the breakdown of the MDD possesses a different shape and symmetry than in the high-field limit. This conclusion is consistent with the result of a recent study of the six-electron system by Maninen *et al.*[14] Kainz *et al.*[21] considered Wigner clusters in parabolic QD's using a multicenter basis in the symmetric gauge. Their vatiational wave function[21] does not allow for formation of the MDD phase, but should be quite equivalent to Eq. (4) in the high-field limit. However, the authors[21] do not discuss the transformations of the Wigner-molecule symmetry.

For the 16-electron system the results depicted in Fig. 3 show that the magnetic field induces several phase transitions. The Wigner molecule created after the breakdown of the MDD possesses the 4-12 shell structure. With the increasing magnetic field the spatial configuration changes first into 5-11 and next into 6-10 structure. Finally, in the high-field regime, the 1-5-10 shell structure is created. Figure 4 shows the charge-density distribution for the four phases of the 16-electron Wigner molecule.

Figure 5 shows the phase diagram calculated for the Wigner molecules with $N=2,\ldots,20$ electrons. We have found that for $N\geqslant 6$ the Wigner molecules undergo several phase transitions until they reach the semiclassical limit[3] of the point-charge structure. This property is related to the fact that—for $N\geqslant 6$—the classical counterpart of the system considered possesses several configurations with nearly the same energy, but different symmetry. It is remarkable that the transitions between different phases of the Wigner molecule show a distinct regularity. At lower magnetic fields, the electrons prefer to occupy the outer shells of the Wigner molecule. If the magnetic field increases, the electron charge-density islands shrink (cf. Figs. 2 and 4) and the more strongly localized electrons can fit into the inner shells of the molecule.

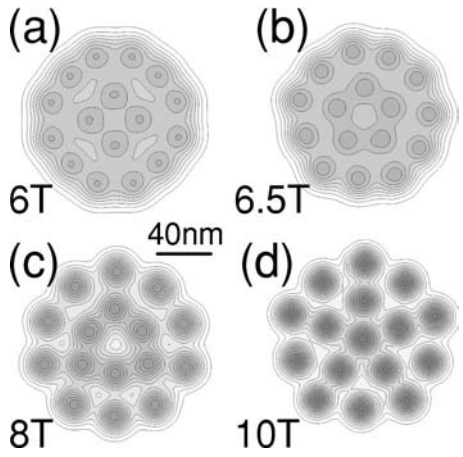


FIG. 4. Electron density distribution for the 16-electron Wigner molecule with shell structure (a) 4-12 for $B=6$ T, (b) 5-11 for $B=6.5$ T, (c) 6-10 for $B=8$ T, and (d) 1-5-10 for $B=10$ T.

In the limit of the infinite magnetic field, the charge distribution associated with Landau orbitals (2) tends towards that of the point charges. The exchange interaction vanishes along with the overlap between the different orbitals. Therefore, in this limit, the shape of the Wigner molecule becomes identical with the shape of its classical counterpart.[3] At lower magnetic field the orbitals are spread out and the overlaps between them do not vanish. In this magnetic-field regime, the shape of the ground-state electron distribution changes due to the finite extension of Landau orbitals (2) and the exchange interaction between the electrons.

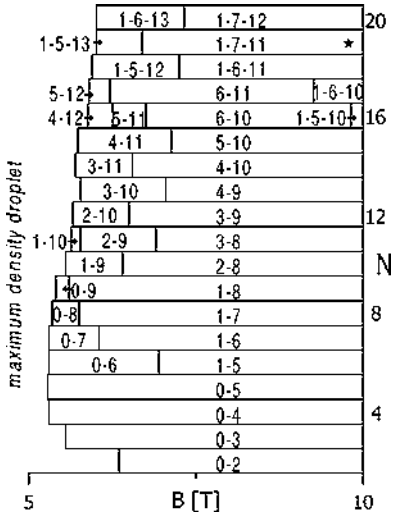


FIG. 5. Phase diagram for $N$-electron Wigner molecules. The lowest-energy shell structures are shown as a function of magnetic field $B$. The boundary of the MDD-stability region is depicted on the left part of the plot. (★) For $N=19$ the 1-6-12 phase appears at $B=15.8$ T.

The instability of the MDD phase under influence of the high magnetic field has been observed experimentally[20] in cylindrical QD's as cusps on the borders of transport windows,[16] which occur when the confined-charge distribution undergoes a reorganization from the MDD into the Wigner molecule. In the present calculations, we have assumed a rotational symmetry of the confinement potential, for which the ground state of the Wigner molecule is degenerate, since the rotation of the system by an arbitrary angle results in energetically equivalent charge distributions. Therefore we can construct the ground state with the rotationally invariant charge-density distribution by taking a superposition of the rotated Wigner-molecule states. The spatial configurations depicted in Figs. 2 and 4, without the rotation symmetry, should be understood in terms of the relative electron-electron distances. However, these lower-symmetry phases can be realized if the rotational symmetry is perturbed, for instance, by a small anisotropy of the confinement potential. In the vertical QD's,[20] the anisotropy is inevitable because of the presence of ionized impurities in the neighborhood of the QD. This anisotropy should stabilize the Wigner-molecule configuration with a fixed space orientation.

In summary, we have presented a systematic study of phase transitions in Wigner molecules induced by an external magnetic field. We have shown that for $N \geqslant 6$ the symmetry of the Wigner-molecule phase, that emerges from the MDD phase, is different than that obtained in the semiclassical, high-field limit. We predict the existence of several phases of the Wigner molecule with different symmetries, that should be observed in the magnetic-field regime above the MDD-breakdown transition. In spite of a qualitative nature of the present results, we suggest the interpretation of the additional cusps on the single-electron-transport plots, observed[20] beyond the MDD stability regime, in terms of the transformations of the Wigner molecules. It is interesting that—contrary to the two-dimensional Wigner crystal, which always posses a fixed (triangular) symmetry—the Wigner molecule can appear in several phases with a different symmetry.

## ACKNOWLEDGMENTS

This paper has been supported by the Polish State Committee for Scientific Research (KBN) under Grant No. 5P03B 4920. One of us (B.S.) gratefully acknowledges the financial support of Foundation for Polish Science (FNP).

[1] L.P. Kouwenhoven, T.H. Oosterkamp, M.W.S. Danoesastro, M. Eto, D.G. Austing, T. Honda, and S. Tarucha, Science **278**, 1788 (1997).
[2] A. Wójs and P. Hawrylak, Phys. Rev. B **53**, 10 841 (1996).
[3] V.M. Bedanov and F.M. Peeters, Phys. Rev. B **49**, 2667 (1994).
[4] R. Price, Z. Xuejun, S. Das Sarma, and P.M. Platzman, Phys. Rev. B **51**, 2017 (1994).
[5] K. Jauregui, W. Häusler, and B. Kramer, Europhys. Lett. **24**, 581 (1993).
[6] P.A. Maksym, H. Imamura, G.P. Mallon, and H. Aoki, J. Phys.: Condens. Matter **12**, R299 (2000).
[7] C.E. Creffield, W. Häusler, S.H. Jefferson, and S. Sarkar, Phys. Rev. B **59**, 10 719 (1999).
[8] R. Egger, W. Häusler, C.H. Mak, and H. Grabert, Phys. Rev. Lett. **82**, 3320 (1999).
[9] S. Akbar and I.-H. Lee, Phys. Rev. B **63**, 165301 (2001).
[10] H-M. Müller and S.E. Koonin, Phys. Rev. B **54**, 14 532 (1996).
[11] M. Taut, Phys. Rev. B **64**, 165315 (2001).
[12] C. Yannouleas and U. Landman, Phys. Rev. B **61**, 15 895 (2000).
[13] S.M. Reimann, M. Koskinen, M. Manninen, and B.R. Mottelson, Phys. Rev. Lett. **83**, 3270 (1999).
[14] M. Manninen, S. Viefers, M. Koskinen, and S.M. Reimann, Phys. Rev. B **64**, 245322 (2001).
[15] B. Reusch, W. Häusler, and H. Grabert, Phys. Rev. B **63**, 113313 (2001).
[16] B. Szafran, S. Bednarek, and J. Adamowski, Phys. Rev. B **65**, 035316 (2002).
[17] A.H. MacDonald, S.R.E. Yang, and M.D. Johnson, Aust. J. Phys. **46**, 345 (1993).
[18] C. deC. Chamon and X.G. Wen, Phys. Rev. B **49**, 8227 (1994).
[19] O. Klein, C. de C. Chamon, D. Tang, D.M. Abusch-Magder, U. Meirav, X.-G. Wen, M.A. Kastner, and S.J. Wind, Phys. Rev. Lett. **74**, 785 (1995).
[20] T.H. Oosterkamp, J.W. Janssen, L.P. Kouwenhoven, D.G. Austing, T. Honda, and S. Tarucha, Phys. Rev. Lett. **82**, 2931 (1999).
[21] J. Kainz, S.A. Mikhalkov, A. Wensauer, and U. Rössler, Phys. Rev. B **65**, 115305 (2002).

INSTITUTE OF PHYSICS PUBLISHING JOURNAL OF PHYSICS: CONDENSED MATTER

J. Phys.: Condens. Matter **15** (2003) 4189–4205 PII: S0953-8984(03)59860-5

# Magnetic-field-induced phase transitions in Wigner molecules

**B Szafran, S Bednarek and J Adamowski**

Faculty of Physics and Nuclear Techniques, University of Mining and Metallurgy (AGH), al Mickiewicza 30, PL-30059 Kraków, Poland

E-mail: adamowski@ftj.agh.edu.pl

Received 21 February 2003, in final form 25 April 2003
Published 6 June 2003
Online at stacks.iop.org/JPhysCM/15/4189

**Abstract**

A theoretical analysis of formation and symmetry transformations is presented for Wigner molecules with $N = 2, \ldots, 20$ electrons confined in quantum dots at high magnetic fields. Using the unrestricted Hartree–Fock method with the multicentre Gaussian basis, we have found that Wigner molecules with $N \geqslant 6$ abruptly change their shape and symmetry with an associated jump in the first derivative of the ground-state energy, i.e. they undergo phase transitions. In particular, the phases of the Wigner molecules obtained just after emerging from the maximum-density droplet (MDD) phase possess a different symmetry from that formed at a high magnetic field. We show that the properties of the electron–electron interaction energy demonstrate very well both the breakdown of the MDD and the quasi-classical character of the Wigner molecule in the high magnetic field. Possible mechanisms of the MDD decay are discussed.

## 1. Introduction

A Wigner phase is a strongly correlated state of the electron system, in which the electrons occupy separate sites forming either a lattice (Wigner crystal) or an island-like structure (Wigner molecule). This quantum electron system with spatially separated electrons exhibits quasi-classical properties. In three-dimensional space, for a low electron density, the phase transition between the electron liquid and crystalline phases was theoretically predicted by Wigner [1]. The formation of a Wigner crystal was observed [2] in the two-dimensional (2D) electron system on the surface of liquid helium. A magnetic-field-induced liquid-to-solid phase transition was reported for a 2D electron plasma at a GaAs/GaAlAs heterojunction [3]. The existence of a pinned Wigner solid was also claimed [4] in Si at zero magnetic field, below a critical electron density. In the ground state, the 2D Wigner crystal forms a triangular (hexagonal) lattice.

Electrons confined in quantum dots (QDs) can form Wigner molecules (also called electronic molecules) [5–8]. Similar to a Wigner crystal in the absence of a magnetic field,

0953-8984/03/244189+17$30.00  

a Wigner molecule is created at low electron density. Application of an external magnetic field yields more favourable circumstances for the creation of a Wigner molecule [6–9]. If the magnetic field increases, the ground state of the electron system confined in the QD undergoes several transformations [10] connected with changes of the spin–orbital configurations and the shape of the electron distribution. For a sufficiently high magnetic field the electrons confined in the QD exhibit complete spin polarization [10]. In this state, called a maximum-density droplet (MDD) [8, 11, 12], the electron density distribution possesses the symmetry of the confinement potential. For a cylindrically symmetric confinement potential the electrons occupy the one-particle states with consecutive magnetic quantum numbers [11, 13]. At higher magnetic fields, the MDD phase decays. The decay of the MDD can be obtained in the framework of the mean-field approaches, i.e. the Hartree–Fock (HF) and local spin density approximation (LSDA) [8]. In the mean-field approaches, the phase that emerges from the MDD does not possess cylindrical symmetry, i.e. it corresponds to the broken-symmetry state. At very high magnetic fields the electrons occupy clearly separated islands forming a Wigner molecule [8, 11, 14]. The Wigner molecule created in the limit of an extremely high magnetic field possesses the same shape as that of a system of classical point charges [16–18]. The breakdown of the MDD has been observed in cylindrical gated QDs [19].

In the literature, different mechanisms of MDD breakdown have been reported. Reimann *et al* [11] interpreted their local-current spin-density results in terms of MDD decay beginning at the edge of the droplet. In this process, a ring of electrons separates out from a flat density maximum [11]. On the other hand, Yang and MacDonald [13] argued that the MDD phase becomes unstable when a hole appears in the electron density in the centre of the QD. In the present paper, we propose a solution to this controversy.

In a recent paper [14], we studied the possibility that Wigner molecules are formed in different space configurations (different phases) [14] and predicted the existence of several new phases of Wigner molecule. In the present paper, we provide the complete results of the calculations performed for the different Wigner molecule phases and an extensive discussion of the underlying physics. The results and discussion presented in this paper considerably extend those given in the brief announcement [14]. Moreover, we discuss the MDD breakdown mechanisms and the applicability of conditions for MDD instability. In the calculations, we have applied the unrestricted HF method with a multicentre basis, which is especially designed for the description of Wigner molecules at high magnetic fields. The proposed basis enables us to describe both the breakdown of the MDD and the quasi-classical localization of the electrons. Using this basis we have studied the behaviour of Wigner molecules with $N = 2, \ldots, 20$ electrons in the magnetic-field regime between the MDD instability and the extremely high-field classical limit.

The paper is organized as follows: section 2 contains the theoretical model and section 3 the results of the calculations of the ground-state energy and electron density distribution. In section 4, we provide a discussion and in section 5 conclusions and a summary.

## 2. Theory

We consider the $N$-electron system confined in a 2D QD and subject to an external magnetic field. We assume that the electrons are spin polarized. The magnetic field $B$ is applied in the $z$ direction and the electrons are confined in the $x$–$y$ plane. In the effective-mass approximation, the Hamiltonian of the system has the form

$$H = \sum_{i=1}^{N}\left(h_i + V_{conf}(r_i) + \sum_{j>i}^{N}\frac{\kappa}{r_{ij}}\right) - \frac{N}{2}g^{\star}\mu_B B, \tag{1}$$

where $h_i$ is the Hamiltonian of a single electron in the magnetic field, $\boldsymbol{r_i} = (x_i, y_i)$, $r_{ij} = |\boldsymbol{r_i} - \boldsymbol{r_j}|$, $\kappa = e^2/4\pi\varepsilon_0\varepsilon$ and $\varepsilon$ is the static dielectric constant. The last term in equation (1) is the Zeeman energy of $N$ spin-polarized electrons, where $g^\star$ is the effective $g$ factor and $\mu_B$ is the Bohr magneton. The QD confinement potential is assumed to be parabolic, i.e.

$$V_{conf}(r) = \tfrac{1}{2}m\omega_0^2 r^2, \tag{2}$$

where $m$ is the electron band mass and $\omega_0$ is the confining frequency. In the non-symmetric (Landau) gauge, the one-particle Hamiltonian for an electron in a magnetic field has the form

$$h = -\frac{\hbar^2}{2m}\left(\frac{\partial^2}{\partial x^2} + \frac{\partial^2}{\partial y^2}\right) + \mathrm{i}\hbar\omega_c y\frac{\partial}{\partial x} + \frac{1}{2}m\omega_c^2 y^2, \tag{3}$$

where $\omega_c = eB/m$ is the cyclotron frequency,

The ground-state energy of Hamiltonian (3), i.e. the lowest Landau level, is equal to $E_0 = \hbar\omega_c/2$. Since this energy level is infinitely degenerate, we can choose the ground-state wavefunction in many forms. We have chosen [14] the one-electron ground-state wavefunction in a form of a displaced Gaussian

$$\psi_{\boldsymbol{R}}(\boldsymbol{r}) = \left(\frac{\alpha}{2\pi}\right)^{1/2} \exp[-(\alpha/4)(\boldsymbol{r} - \boldsymbol{R})^2 + (\mathrm{i}\alpha/2)(x - X)(y + Y)], \tag{4}$$

where $\boldsymbol{R} = (X, Y)$ is an arbitrary vector and $\alpha = eB/\hbar$. One can easily prove that wavefunction (4) fulfils the eigenequation for Hamiltonian (3) with eigenvalue $E_0$. The electron density distribution associated with wavefunction (4) has the shape of the Gaussian centred at point $\boldsymbol{R}$, which can be treated as the centre of the Landau orbit of the single electron.

In the present paper, wavefunctions (4), centred at different $\boldsymbol{R} = \boldsymbol{R}_i$, are used to form the multicentre variational basis, which is suitable for a description of Wigner molecules. A similar approach, but with the one-electron wavefunctions written in the symmetric gauge, was applied to Wigner crystals [20, 21] and Wigner molecules [22, 23]. We solve the $N$-electron eigenproblem by the unrestricted HF method with the one-electron wavefunctions

$$\Psi_\nu(\boldsymbol{r}) = \sum_{i=1}^{N} c_i^\nu \tilde{\psi}_{\boldsymbol{R}_i}(\boldsymbol{r}), \tag{5}$$

where $\nu$ numbers the occupied one-electron states ($\nu = 1, \ldots, N$), $c_i^\nu$ are the linear variational parameters and $\tilde{\psi}_{\boldsymbol{R}_i}(\boldsymbol{r})$ are taken in the form of (4) with the parameter $\alpha$ replaced by the nonlinear variational parameter $\alpha^\star$. In order to determine the positions of $N$ centres $\boldsymbol{R}_i$ in wavefunction (5), we consider the classical counterpart of the Wigner molecule, i.e. the system of $N$ classical equally charged particles confined in potential (2). The total potential energy of this classical system is given by

$$U_{tot}^c = \sum_{i=1}^{N}\left(V_{conf}(R_i^c) + \sum_{j>i}^{N}\frac{\kappa}{|\boldsymbol{R}_i^c - \boldsymbol{R}_j^c|}\right), \tag{6}$$

where $\boldsymbol{R}_i^c$ are the position vectors of $N$ classical point charges in the configuration, for which potential energy (6) possesses a local minimum. In the quantum-mechanical calculations, we apply the following scaling of the centres of Gaussians: $\boldsymbol{R}_i = \sigma\boldsymbol{R}_i^c$, where the scaling factor $\sigma$ is the second nonlinear variational parameter. For the sake of feasibility of the present calculations we have applied uniform scaling of the classical configurations instead of introducing separate variational parameters in the wavefunctions (5). This choice enables us to reproduce the classical configurations in the limit of the infinite magnetic field, for which the charge distribution associated with wavefunction (5) tends to that of the classical point charges.

**Table 1.** Ground-state energy of the 2D two-electron system in parabolic confinement for different magnetic fields $B$. We quote the results $E_{exact}$ of the exact calculations, the HF estimates $E_{HF}$, and their difference $\Delta E$. Energy is expressed in meV.

| $B$ (T) | $E_{exact}$ | $E_{HF}$ | $\Delta E$ |
|---|---|---|---|
| 3 | 13.02 | 13.34 | 0.32 |
| 5 | 15.77 | 15.90 | 0.23 |
| 10 | 23.35 | 26.97 | 0.43 |
| 20 | 39.88 | 40.10 | 0.22 |
| 30 | 56.71 | 56.84 | 0.13 |

In the present paper, basis (5) contains, besides two nonlinear variational parameters $\alpha^\star$ and $\sigma$, $N$ complex linear parameters $c_i^\nu$ for each electron, i.e. $N^2$ parameters for the $N$-electron system. However, taking into account that the linear parameters are not entirely independent, since in the HF method wavefunctions $\Psi_\nu$ are forced to be mutually orthogonal, we have at our disposal $N(N+1)/2$ independent linear variational parameters.

## 3. Results

Throughout the present paper, we apply the notation of different space configurations of Wigner molecules, which stems from the classical charge system [16–18]. Accordingly, we denote by $N_1$–$N_2$–$N_3$ the configuration of the $N$-electron Wigner molecule in which the inner, middle and outer shells are occupied by $N_1$, $N_2$ and $N_3$ electrons, respectively, whereby $N = N_1+N_2+N_3$. In the case of only two occupied shells, we label the corresponding configuration by $N_1$–$N_2$ and omit zero for the unoccupied outermost shell. This notation corresponds to the shell-like equilibrium configuration of equally charged classical particles [16–18].

In the calculations, we have used the material parameters of GaAs, i.e. $m = 0.067\ m_e$, $\varepsilon = 12.9$, $g^\star = 0.54$ and $\hbar\omega = 3$ meV. It is known that the HF method works with a relatively high precision for spin-polarized electron systems [12, 15], which are considered in the present paper. In a recent paper [14] we performed test calculations in order to check the quality of basis (5) in the high-magnetic-field regime, i.e. for $B = 20$ T. We have shown [14] that the Slater determinant constructed from wavefunctions (5) leads to the results close to the those of Müller and Koonin [6], which were obtained in a symmetric gauge with the definite angular momentum basis. For $N \geqslant 4$ the present upper bounds are better than those of [6]. We note that in our approach only one element of basis (5) is needed for each electron. Therefore, the present method requires much less computational effort than the method used in [6], in which a superposition of a large number of angular momentum eigenstates is necessary in order to reproduce the localized island-like distribution of electrons. We have also compared our results with those obtained using the Monte Carlo method [24] and found a good agreement. Moreover, we have estimated the precision of the present approach by applying it to the two-electron system with 2D parabolic confinement. In this case, the eigenproblem is separable into centre-of-mass and relative-coordinate problems, which can be solved exactly [25]. A comparison of the present HF estimates with the exact results [25] is given in table 1. The results quoted in table 1 show that the HF inaccuracy does not exceed 0.5 meV, reaches a maximum for $B = 10$ T, and then decreases with the magnetic field.

These test calculations verify the reliability of the present computational method in the magnetic-field regime considered. The high precision of the present calculations in the high-magnetic-field limit results from the fact that, in this regime, basis (5) allows us to reproduce the properties of classical Wigner molecules. However, some improvement of the present results is possible for lower magnetic fields. In order to enable the reader to verify the accuracy of the

**Table 2.** Energy (in meV) of the different phases of the Wigner molecules with $N = 4, 6, 9$, and 16 electrons for several values of the external magnetic field. The notation of Wigner-molecule phases is defined in the text.

| $B$ (T) | 0–4 | 0–6 | 1–5 | 1–8 | 2–7 | 5–11 | 1–6–11 |
|---|---|---|---|---|---|---|---|
| 6 | 52.01 | 99.88 | 100.06 | 193.16 | 193.33 | 496.28 | 496.39 |
| 10 | 64.00 | 118.45 | 117.98 | 220.62 | 220.40 | 545.67 | 545.60 |
| 16 | 83.23 | 147.20 | 146.58 | 263.36 | 263.04 | 620.64 | 620.36 |
| 30 | 129.88 | 216.88 | 216.34 | 367.55 | 367.29 | 804.71 | 804.48 |

present approach, we list in table 2 the total energies of the 4-, 6-, 9- and 16-electron Wigner molecules in different phases.

The results for the six-electron system are displayed in figure 1, which shows the dependence of the ground-state energy on the magnetic field calculated with wavefunction (5) for the MDD and Wigner molecules in configurations 0–6 and 1–5. For the spin-polarized MDD phase the results of the restricted HF method cannot be amended by the unrestricted version of the HF method. For the MDD it is more convenient to use the symmetric gauge, since the optimal one-electron wavefunctions are the eigenstates of the single-electron operator of the $z$ component of the angular momentum. In order to perform an additional test of the present method, we have solved the restricted HF equations by the numerical finite-difference method for the cylindrically symmetric MDD phase. This numerical approach takes into account the full cylindrical symmetry of the MDD phase and yields results that are exact within the HF approach. In figure 1, we compare these accurate results (dotted curve) with those obtained with the multicentre basis (5) (solid and dashed curves). In the MDD stability regime, the results of the calculations with the two different multicentre bases (5) slightly overestimate the exact MDD energy, but run parallel and close to the accurate curve. Moreover, both the bases, which correspond to the configurations 0–6 and 1–5, work with the same precision in the MDD regime. In the insets of figure 1, the ground-state electron density distributions are depicted. All the electron distributions, including that for the MDD phase, have been obtained with basis (5). We see that the multicentre wavefunction (5) describes the localized island-like distribution of electrons in the molecular phases and moreover reproduces surprisingly well the cylindrically symmetric electron distribution in the MDD phase.

For $B \simeq 5$ T the curves obtained with the multicentre basis (5) rapidly change their slope. Then, the charge distribution obtained with basis (5) ceases to mimic the MDD and goes over into the molecular type of localization. At this field, the energies of the 0–6 and 1–5 Wigner molecules become lower than the MDD energy. Just after the breakdown of the MDD the 0–6 phase possesses the lowest energy. However, at higher magnetic fields the 1–5 configuration becomes the lowest-energy phase. The appearance of this phase can be predicted based on the properties of the classical Wigner molecule, since the 1–5 configuration is the lowest-energy configuration of the six-electron classical Wigner molecule and the classical limit is reached at infinite magnetic field. These results indicate that the phase of the six-electron system changes first from the MDD into the 0–6 molecular phase, and next from the 0–6 into the 1–5 phase.

The determination of the critical magnetic field for MDD breakdown is rather ambiguous. In our previous paper [14] we used one possible approach, i.e. we found the magnetic field for which the energy estimate obtained with the multicentre basis becomes lower than the exact MDD energy. However, this approach overestimates the critical magnetic field, since the MDD energy is exact (within the HF method), while the upper bounds obtained with the multicentre basis (5) can be improved in the finite-magnetic-field regime. In the present paper, we also search for the critical magnetic field using another approach, which exploits only the

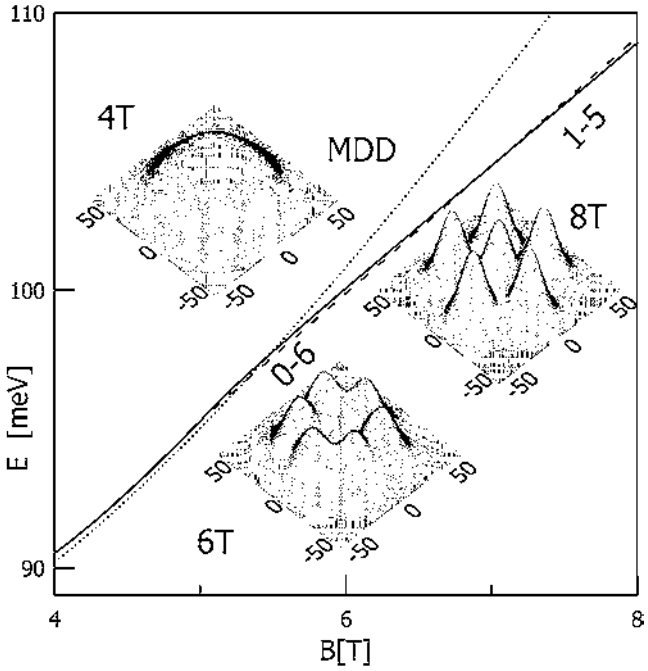


**Figure 1.** Ground-state energy $E$ of the six-electron MDD (dotted curve) and the Wigner molecule in phases 0–6 (solid curve) and 1–5 (broken curve) as functions of magnetic field $B$. Insets show the corresponding electron density distributions on the $x$–$y$ plane (length is measured in nanometres).

results obtained with basis (5). When comparing the energy estimates calculated by the same method, the possible errors cancel out, which justifies this approach. Moreover, the charge density distribution obtained with basis (5) mimics that of the MDD phase in the magnetic-field regime below the critical field for the MDD/Wigner molecule transition and yields the molecular charge distribution above the critical field.

In the present paper, instead of comparing the ground-state energies, which differ by a small amount (cf figure 1), we use the characteristic properties of the electron–electron interaction energy to extract the critical magnetic field. Figure 2 displays the expectation value of the total electron–electron interaction energy, which is defined as follows:

$$E_{int} = \langle \Phi | \sum_{i=1}^{N} \sum_{j>i}^{N} \frac{\kappa}{r_{ij}} | \Phi \rangle, \tag{7}$$

where $\Phi$ is the Slater determinant constructed from the orthogonal one-electron eigenfunctions of the HF operator obtained with basis (5). In figure 2, the magnetic-field regime to the left of the peak position corresponds to the MDD phase. The increase of the magnetic field in the MMD regime forces the electron charge distribution to shrink. As a result, in this magnetic-field regime, the electron–electron interaction increases with increasing magnetic field. At a certain magnetic field, the electron–electron repulsion becomes so strong that the MDD breaks down and the charge distribution undergoes reorganization into an island-like molecular configuration. In the molecular phase, the electron–electron interaction energy rapidly decreases. Therefore, the critical magnetic field for the breakdown of the MDD phase can be precisely determined from the position of the sharp peak on the interaction energy versus magnetic field plot (cf figure 2). The critical magnetic fields determined in such a way are equal

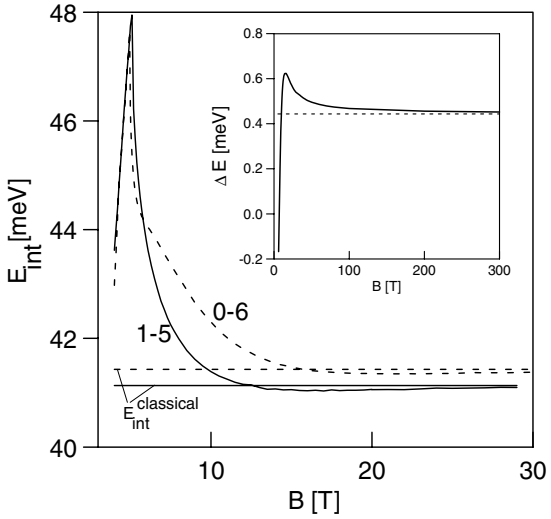


**Figure 2.** Expectation value $E_{int}$ of the total electron–electron interaction energy (equation (7)) for the six-electron system confined in the QD as a function of magnetic field $B$. Solid (broken) curve shows the results obtained with wavefunction (5) corresponding to configuration 1–5 (0–6). The electron–electron interaction energy $E_{int}^{classical}$ is shown by the horizontal lines for classical molecules 1–5 (solid curve) and 0–6 (broken curve). Inset: energy difference $\Delta E$ between the ground-state energies of the 0–6 and 1–5 Wigner molecule phases. The horizontal broken line shows this energy difference for the classical Wigner molecule.

to 4.9 and 5.1 T, for the decay of the MDD into the 0–6 and 1–5 molecular phases respectively, which means that the 0–6 phase of the Wigner molecule is formed just after the breakdown of the MDD. The 0–6 phase has the lowest energy up to 6.95 T (cf figure 1). Above the MDD breakdown, the electron–electron interaction energies for both molecular phases decrease with increasing magnetic field, pass through flat minima and approach the corresponding high-field limit values from below. The horizontal lines in figure 2 mark the values of the electron–electron interaction energy for classical Wigner molecules (cf the second term in equation (6)). In the high-field limit, the quantum-mechanical expectation values asymptotically reach the corresponding classical values, which is another signature of the classical behaviour of the system at extremely high magnetic fields. The electron–electron interaction energy turns out to be a useful quantity for demonstrating both the MDD breakdown and the quasi-classical properties of the electrons in the high-magnetic-field limit. We have found that the plots of the interaction energy versus magnetic field $B$ are qualitatively the same for all $N$.

The inset of figure 2 shows the difference $\Delta E$ of the energies of the 1–5 and 0–6 phases as a function of the magnetic field. The difference between the energies of the corresponding classical Wigner molecules is equal to 0.44 meV. We see that $\Delta E$ is maximal for $B \simeq 15$ T. At higher magnetic fields, $\Delta E$ decreases and approaches its classical limit value. The convergence to the classical value is slow and the limit is reached at infinite magnetic field.

Figure 3 shows the results for the ground-state configurations of the Wigner molecules with $N = 2, \ldots, 20$ electrons. We mark the different phases of the Wigner molecules by symbols $\alpha_i$, $\beta_i$ and $\gamma_i$, where $\alpha_i$ stands for the 0–$i$ phase with $i = N$, $\beta_i$ denotes the $i$–$(N - i)$ phase and $\gamma_i$ denotes the phase 1–$i$–$(N - i - 1)$. The critical magnetic fields for the transformations between the different phases of the $N$-electron system confined in the QD can be found from the positions of the horizontal lines in figure 3. The uppermost horizontal solid lines show the critical magnetic fields for the formation of the Wigner molecule determined from the

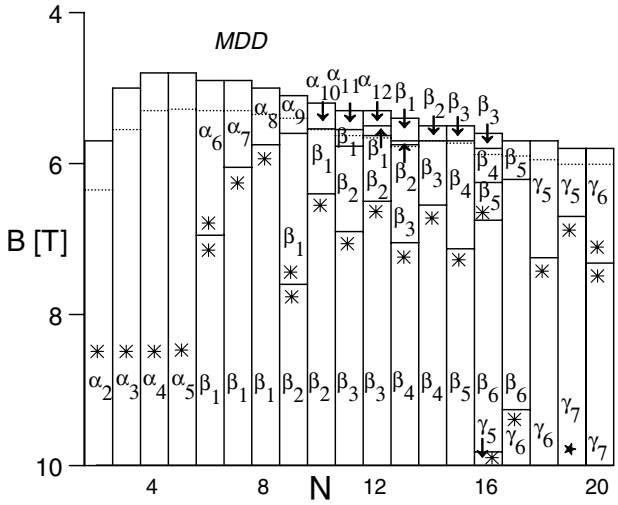


**Figure 3.** Phase diagram for Wigner molecules. The MDD decay and formation of different Wigner molecule phases is shown as a function of external magnetic field $B$ and the number $N$ of electrons. The uppermost horizontal solid lines correspond to the critical magnetic fields for the MDD decay, determined according to condition (I), described in the text. The horizontal dotted lines correspond the critical magnetic fields, determined by condition (II). The different phases of the Wigner molecules are marked by symbols $\alpha_i$, $\beta_i$ and $\gamma_i$, where $\alpha_i$ denotes the 0–$i$ configuration with $i = N$, $\beta_i$ the $i$–$(N-i)$ configuration, and $\gamma_i$ the 1–$i$–$(N-i-1)$ configuration. The asterisks denote the phases for which the configuration of the Gaussian centres in basis (5) have been taken as the scaled classical configuration corresponding to the local minima of the potential energy. Other phases (without asterisks) have been obtained with the use of the additional Gaussian repulsive core (equation (8)). ($\star$) For $N = 19$ the 1–6–12 configuration becomes the ground state of the electron system at $B = 15.8$ T.

peak positions of the electron–electron interaction energy (cf figure 2), i.e. according to the condition which in the following will be referred to as condition (I). The dotted horizontal lines correspond to the values of the magnetic field for which the ground-state energy calculated with the multicentre basis becomes lower than the exact HF result for the MDD phase (cf figure 1), i.e. according to the condition which will be referred to as condition (II). In our previous paper [14] we used only condition (II) to determine the MDD breakdown. In figure 3 the following new phases, $\alpha_{10}$, $\alpha_{11}$, $\alpha_{12}$, $\beta_1$, $\beta_2$ and $\beta_3$, appear for $N = 10, \ldots, 16$ in the range of magnetic fields for which condition (I) is fulfilled and condition (II) is not yet fulfilled. These new phases were absent in the phase diagram of [14].

The difference between the values of the critical magnetic fields determined according to conditions (I) and (II) decreases with increasing number of electrons. For example, this difference is equal to 0.7 T for $N = 2$ and 0.2 T for $N = 20$. The critical magnetic fields, determined according to condition (I) seem to be more reliable, since when applying condition (I) we are using the same method in order to estimate both the MDD and Wigner molecule energies, i.e. the errors cancel out. The critical fields derived according to condition (II) result from a comparison of the energy estimates obtained by the two different methods with different accuracies.

According to figure 3, the Wigner molecule with $N \geqslant 6$ electrons possesses at least two different ground-state configurations (phases). Each of these phases has the lowest energy in different magnetic-field regimes. For $N = 11, \ldots, 16$ electrons the Wigner molecule phase emerging from the MDD and determined by condition (I) is replaced by another phase

before condition (II) is fulfilled. The Wigner molecule phases marked by asterisks in figure 3 have been obtained using the positions of the centres of Gaussians (4) taken from the scaled classical configurations obtained with the parabolic confinement potential. Nevertheless, not all the configurations corresponding to the quantum ground state can be obtained with purely parabolic confinement. In particular, the phases which appear just after the MDD breakdown, and which correspond to the electrons gathering at the outer ring of the molecule, have to be found by another method. In order to obtain the classical configurations for these phases of the Wigner molecules, i.e. those not marked by the asterisks in figure 3, we have introduced into the confining potential a weak Gaussian repulsive core

$$U_{rep} = V_0 \sum_{i=1}^{K} \exp[-(R_i^c/R_0)^2], \tag{8}$$

which acts on a limited number $K$ of electrons. The repulsive core (8) induces the formation of those molecules with a larger number of electrons on the outer ring. In the calculations we have used $R_0 = 30$ nm, $V_0 \in [2, 5]$ meV and $K = N$ for phases $\alpha_i$, $K = N - i$ for phases $\beta_i$, and $K = N - i - 1$ for phases $\gamma_i$.

Figure 4 displays the results for the 10-electron MDD and for the 0–10, 1–9 and 2–8 phases of the Wigner molecules. The energy is calculated with respect to the energy of the 2–8 phase, which corresponds to the ground state in the high-magnetic-field limit. Crossing points (a), (b) and (c) show the values of the critical fields corresponding to the phase transitions. Point (a) corresponds to the breakdown of the MDD, obtained from condition (I). At this magnetic field, the charge densities obtained with the multicentre bases go over into the molecular-type charge densities. Above point (a), the ground-state energies, calculated with wavefunction (5) for the 0–10, 1–9 and 2–8 configurations, become different. The 0–10 configuration possesses the lowest energy up to point (b). At point (b), the ground-state energy obtained with the 0–10 and 1–9 multicentre bases crosses with the MDD energy, i.e. at this point condition (II) of the MDD breakdown is fulfilled. Moreover, the ground-state Wigner molecule changes its shape and above point (b) becomes the 1–9 configuration. Point (c) corresponds to the transition between the 1–9 and 2–8 Wigner molecule phases. The evolution of the 10-electron density distribution depicted in the insets of figure 4 indicates that the MDD decays from the centre with the formation of a hole in the electron density (cf phase 0–10). This result is compatible with the MDD breakdown mechanism proposed by Yang and MacDonald [13].

For the Wigner molecules with $N \leqslant 20$, considered in the present paper, we have found that the largest number of different phases appears for $N = 16$. According to figure 3, the 16-electron Wigner molecule can occur in five (four according to condition (II)) different phases, which are stable in different magnetic-field regimes. The energy of these phases calculated with respect to the energy of the high-field 1–5–10 phase is displayed in figure 5. The Wigner molecule occurs in phases 3–13, 4–12 and 5–11 at $B = 5.6, 5.8$ and 6.25 T respectively. We note that the transition of the 16-electron Wigner molecule into its ultimate phase 1–5–10, which corresponds to the classical equilibrium configuration, appears at particularly high magnetic field $B = 9.8$ T. This is apparently due to the fact that the classical 16-electron molecule is the one in which the third ring is formed.

Figures 6 and 7 display the electron density distributions for $N = 16$ and 20 respectively. We note that in the 1–6–13 configuration of the 20-electron Wigner molecule created just after the breakdown of the MDD (cf figure 7 for $B = 6$ T) the maxima of the electron density located on the outermost shell are much more pronounced (sharper) than those located on the inner shells. In figures 6 and 7, the contour lines introduced for $B = 6$ T correspond to the values of the charge density close to the maxima. We note that the maxima near the centre of the charge distribution are flatter and possess a larger spatial extension than those at the

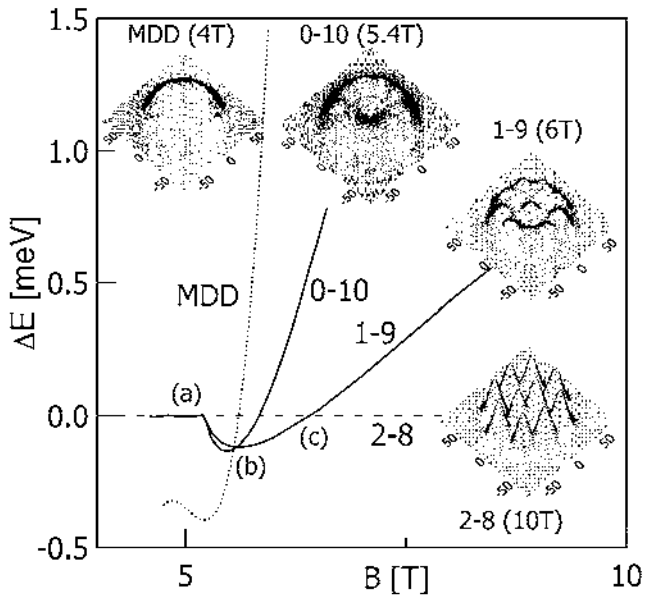


**Figure 4.** Energy difference $\Delta E$ between the ground-state energies of the different phases for the 10-electron system confined in the QD and the ground-state energy of the high-field 2–8 phase (broken horizontal line) as a function of magnetic field $B$. The dotted curve shows the results for the MDD and the solid curves show the results for the Wigner molecules in phases 0–10 and 1–9. Insets show the corresponding electron density distributions on the $x$–$y$ plane (length is measured in nanometres). Points (a), (b) and (c) are described in the text.

edge. This is a trace of the MDD breakdown mechanism via edge reconstruction [11]. We will discuss this mechanism in section 4. At higher magnetic fields, all the electron density maxima are equally sharp (cf figure 7 for $B = 8$ and 12 T).

## 4. Discussion

The results of the present calculations show that in the external magnetic field the Wigner molecules undergo several ground-state transformations. Each of these transformations is associated with a discontinuity of the first derivative of the ground-state energy (cf figures 1, 4 and 5) and a rapid change of the spatial symmetry of the electron density distribution. Therefore, we can treat these transformations as phase transitions in a few-electron system.

We have found that a Wigner molecule with six or more electrons can appear in more than one phase. The transitions between these phases, induced by the magnetic field, exhibit a certain regularity. In the Wigner molecule phase formed from the MDD, the electrons prefer to occupy the outer shells. For $N = 6, \ldots, 12$ ($N = 6, \ldots, 10$ according to condition (II)) the molecular phases that emerge from the MDD consist of a single ring of electrons, while the quasi-classical, high-field phases are composed of two rings. However, for $N = 13, \ldots, 17$ ($N = 11, \ldots, 17$ according to condition (II)) the molecules formed from the MDD are composed of two rings, while the high-field phases consist of three rings. At higher magnetic fields, the larger number of electrons starts to occupy the inner and middle shells. In the infinite magnetic field limit, the space configuration of the electron distribution islands in the Wigner molecule exactly corresponds to the equilibrium configuration of the classical charge carriers. For finite magnetic fields, the average interelectron distances in the quantum and classical systems are different.

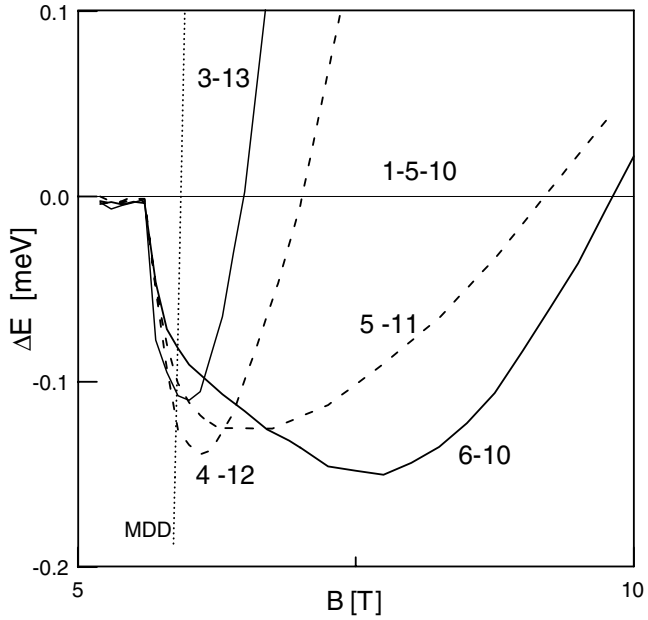


**Figure 5.** Energy difference $\Delta E$ between the ground-state energy of the 16-electron system confined in the QD and the ground-state energy of the high-field 1–5–10 phase (thin horizontal line) as a function of magnetic field $B$. The dotted curve shows the results for the MDD, the solid curves show the results for the Wigner molecule in 3–13 and 6–10 phases, and broken curves—for 4–12 and 5–11 phases.

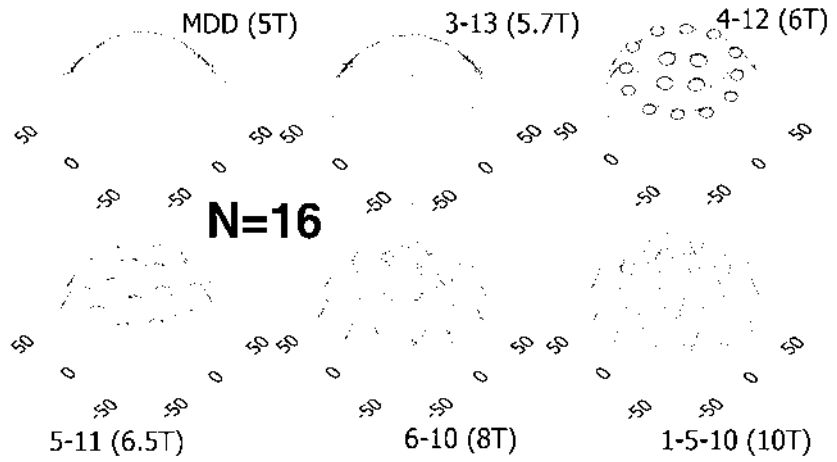


**Figure 6.** Electron density distribution on the $x$–$y$ plane for $N = 16$ electrons for several magnetic fields. Contour lines drawn for $B = 6$ T correspond to the electron density close to the maximum. Length is measured in nanometres.

Only in the limit $B \longrightarrow \infty$ do the average interelectron distances in the quantum Wigner molecule become the same as those in the classical charge carrier system. Therefore, the application of a high magnetic field to the electron system confined in a QD allows us to observe a continuous transition from quantum mechanical to classical behaviour.

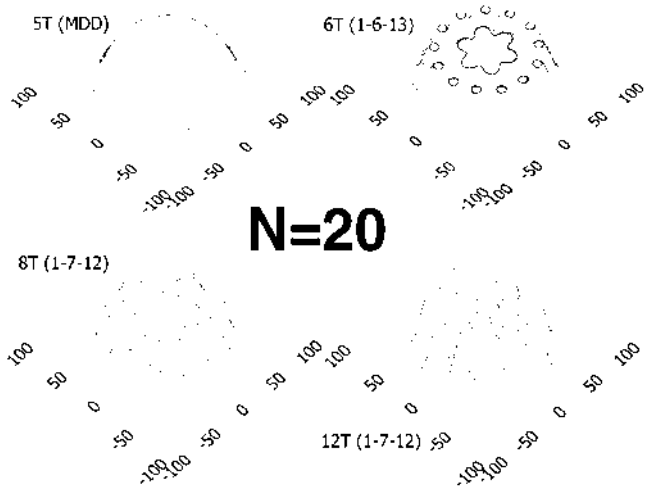


**Figure 7.** Electron density distribution on the $x$–$y$ plane for $N = 20$ electrons for several magnetic fields. Contour lines drawn for $B = 6$ T correspond to the electron density close to the maximum. Length is measured in nanometres.

In order to get a deeper insight into the physics of Wigner molecules we have considered the different contributions to the ground-state energy. Figure 8 shows the expectation value of the Coulomb interaction energy,

$$\langle V_C \rangle = \int \mathrm{d}^2 r_1 \, \mathrm{d}^2 r_2 \, \frac{\kappa}{R} |\psi_{\boldsymbol{R}_1}(\boldsymbol{r}_1)|^2 |\psi_{\boldsymbol{R}_2}(\boldsymbol{r}_2)|^2, \tag{9}$$

calculated with ground-state wavefunctions (4) centred at $\boldsymbol{R}_1 = (0, 0)$ and $\boldsymbol{R}_2 = (0, R)$ for fixed $\alpha^\star = \alpha = eB/\hbar$ with $B = 6$ T. This energy is equal to the Hartree energy of the interaction between the two electrons with Gaussian wavefunctions (4). We notice that, contrary to the Coulomb interaction potential $\kappa/R$, the interaction energy $\langle V_C \rangle$ is non-singular at $R = 0$, i.e. the interaction energy of the two spread charges is finite, in contrast to the interaction energy of the two point charges. If the distance between the centres of two Gaussians (4) exceeds $\sim$15 nm, the Hartree energy becomes larger than $\kappa/R$. At large distances, $\langle V_C \rangle$ goes over into $\kappa/R$. In figure 8, we have also depicted the exchange integral

$$\langle E_X \rangle = \int \mathrm{d}^2 r_1 \, \mathrm{d}^2 r_2 \, \frac{\kappa}{R} \psi^*_{\boldsymbol{R}_1}(\boldsymbol{r}_1) \psi_{\boldsymbol{R}_2}(\boldsymbol{r}_1) \psi^*_{\boldsymbol{R}_2}(\boldsymbol{r}_2) \psi_{\boldsymbol{R}_1}(\boldsymbol{r}_2). \tag{10}$$

For $R = 0$ the exchange and Hartree energies take on the same values. The exchange energy rapidly decreases with $R$ and becomes equal to zero, when the overlap between functions $\psi_{\boldsymbol{R}_1}$ and $\psi_{\boldsymbol{R}_2}$ vanishes. For $R \gtrsim 50$ nm, the two Gaussian charge distributions interact as the classical point charges. At higher magnetic fields, this effective interaction becomes classical for smaller separations between the centres of the Gaussians.

Figure 9 displays the magnetic-field dependence of the nonlinear variational parameters $\alpha^\star$ and $\sigma$ in wavefunction (5) with configurations of the centres corresponding to the classical molecule (phase 1–5). Figure 9(a) shows the variational parameters in the magnetic-field regime that corresponds to the molecular phase ($B > 5.1$ T). We note that above the MDD breakdown both $\sigma$ and $\alpha^\star/\alpha$ are larger than 1. In the Wigner molecules the distances between the centres of the electron localization are of the order of 30 nm. For these distances the mutual electrostatic repulsion between the Gaussian charge distributions is stronger than the repulsion

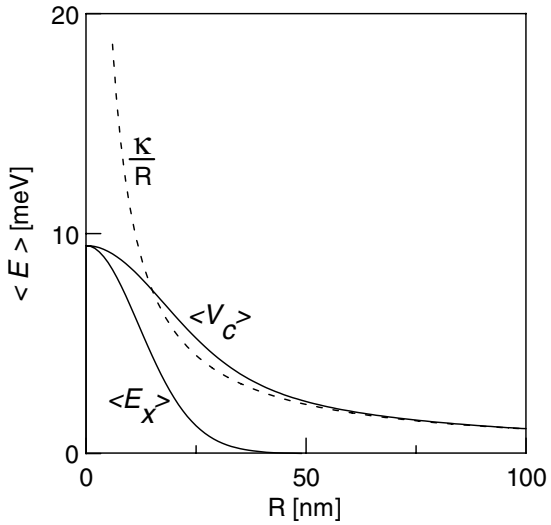


**Figure 8.** Expectation values of the Hartree energy $\langle V_C \rangle$ (equation (9)) and exchange energy $\langle E_X \rangle$ (equation (10)) as functions of interelectron distance $R$. The Coulomb interaction potential energy is shown by the dashed curve.

between point charges. Since $\sigma > 1$, the quantum Wigner molecule possesses a slightly larger size than its classical counterpart. Moreover, in the Wigner molecule $\alpha^\star > \alpha$, which means that the Gaussian charge distributions shrink as a result of the interelectron repulsion. In the magnetic-field regime, in which the transitions between different Wigner molecule phases appear, the nonlinear variational parameters deviate considerably from their high-field values (cf figure 9(a) for small $B$). On the other hand, in the classical high-field limit $\alpha^\star \longrightarrow \alpha$, i.e. the Gaussian electron distribution goes over into a delta-like electron localization, and $\sigma \longrightarrow 1$, i.e. the electron configuration goes over into that of the classical charge system.

Figure 9(b) shows the changes in the variational parameters in the region of the MDD/Wigner molecule phase transition. The scaling parameter $\sigma$ takes on a much lower value ($\sim$0.6) for the MDD phase and rapidly jumps when the MDD decays and the molecular phase is formed. The parameter $\alpha^\star$ exhibits a small jump at the MDD/Wigner molecule phase transition.

Wavefunction (5) with the two variational parameters $\alpha^\star$ and $\sigma$ is sufficiently flexible to reproduce the properties of both the MDD and molecular phases. In the present HF method, the Slater determinant is constructed from the orthogonalized wavefunctions constructed in basis (5). Kainz *et al* [22] applied the symmetric-gauge form of wavefunction (4) with only one variational parameter $\sigma$. In [22], the Slater determinant was constructed from the non-orthogonal one-electron wavefunctions. Because of this non-orthogonality, the approach of Kainz *et al* [22] is not equivalent to the HF method at finite magnetic fields. In particular, this approach [22] fails to reproduce the MDD phase, which is probably caused by the fact that every element of the Slater determinant is only one function of type (4), but not a superposition of many such functions as in the present approach. Moreover, the authors [22] found only minima of the total energy corresponding to the scaling parameter $\sigma > 1$, while in the present calculations the MDD phase is obtained if $\sigma$ is much smaller than 1. In the high-field limit, orbitals (4) become orthogonal due to the lack of the overlap. Then, both the present method and the approach of Kainz *et al* [22] work with the same precision.

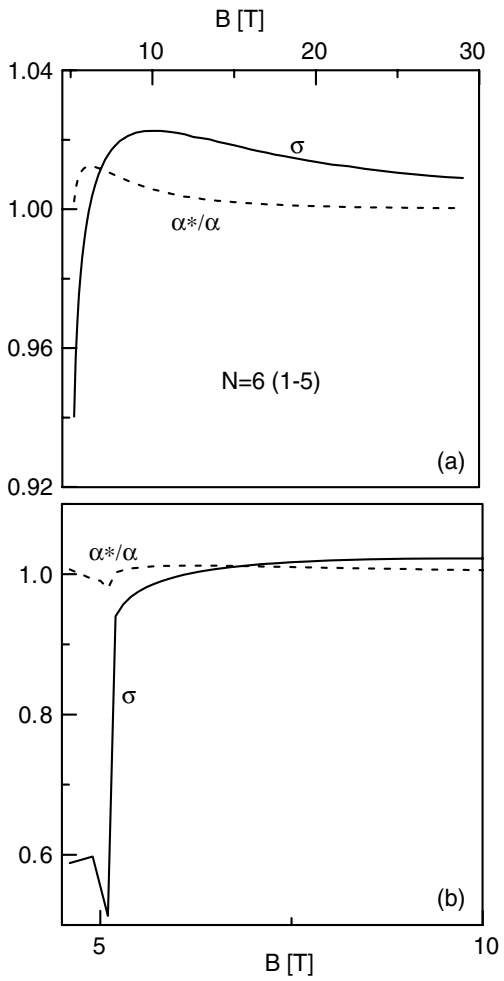


**Figure 9.** Nonlinear variational parameters $\alpha^\star$ and $\sigma$ versus external magnetic field $B$ for $N = 6$ obtained with the 1–5 multicentre basis. (a) The results for the Wigner molecule magnetic-field regime. (b) The results for the magnetic-field regime near the MDD breakdown.

The instability of the MDD and the formation of a broken-symmetry phase of the Wigner molecule in QDs was considered in [9, 11, 26–28]. The crossover from the Fermi liquid to the Wigner molecule behaviour was studied both in the absence [26–28] and in the presence [9, 11, 13, 29] of a magnetic field. In [9, 26–28], only a single phase of the Wigner molecule was found. Manninen *et al* [29], using an exact diagonalization scheme, found the ground state in the 0–6 configuration in the intermediate magnetic-field regime. In the present paper we have found a similar effect.

Yang and MacDonald [13] obtained a redistribution of the electrons over the orbitals with different angular momenta. They interpreted their results in terms of the holes, which arise in the occupation number distribution. The occupation number distribution [13] cannot be unambiguously translated into the spatial distribution of electrons, considered in the present paper. According to the results of [13], the decay of the MDD for $N = 2, \ldots, 14$ is accompanied by one electron missing in the zero angular momentum state, which—in terms

of the spatial electron distribution—means that the MDD decays from its centre with the electrons gathering at the outer surface. This interpretation agrees with the results of the present calculations. The results of the exact diagonalization performed by Manninen *et al* [29] for the six-electron system also confirm this mechanism of the MDD breakdown.

However, Reimann *et al* [11], based on the results of the density functional approach, suggest another mechanism for MDD breakdown via edge reconstruction [30]. According to this mechanism, the MDD undergoes a transition into the Wigner molecule gradually, when the cylindrically symmetric electron distribution of the MDD starts to break down from the edge. Then, a ring of separately localized electrons emerges from the central flat maximum of the electron distribution. The present results contradict this mechanism for $N < 12$. However, in our opinion, edge reconstruction can indeed occur for a larger number of electrons. In particular, the plots of the charge distribution presented in figures 6 and 7 indicate that during the MDD breakdown the maxima corresponding to the electrons localized at the edge of the electron distribution are sharper than the maxima corresponding to the electrons localized near the centre of the QD. Therefore, based on the present results, we suggest that the MDD starts to decay from the central part for $N \leqslant 12$ and from the edge for $N > 12$. Moreover, it is not excluded that the MDD with fewer electrons decays via simultaneous central hole formation and edge reconstruction.

Experimental evidence for the instability of the MDD phase was reported by Ooesterkamp *et al* [19]. They measured the single-electron transport through a cylindrical gated QD in a magnetic field and observed cusps on the plots, which determine the boundaries of the transport windows [10]. The conditions of the single-electron tunnelling are determined by the energy balance between the QD chemical potential ($\mu_N$) and electrochemical potentials of the leads [10]. Since $\mu_N = E_{N+1} - E_N$, where $E_N$ is the ground-state energy of the $N$-electron system confined in the QD, the cusps of the function $\mu_N(B)$ are connected with the cusps of $E_N(B)$, i.e. they result from the magnetic-field-induced phase transitions. The additional cusps were observed [19] at magnetic fields higher than those corresponding to the MDD breakdown. Based on the present results, we suggest that these additional transitions [19] can be interpreted as the phase transitions between the different phases of the Wigner molecules. A direct experimental observation of the different electron spatial localizations in the different Wigner molecule phases requires another type of measurement, e.g. wavefunction mapping [31].

## 5. Conclusions and summary

The present calculations have been performed under the assumption of rotational symmetry of the QD confinement potential. The mean-field approaches lead inevitably to the broken-symmetry solutions for the Wigner phase [8]. Cylindrical symmetry can be conserved by the charge distribution calculated with the exact diagonalization schemes for the Wigner phase [13, 29]. The present broken-symmetry distributions should be understood in terms of the relative electron–electron positions. The rotation of the broken-symmetry electron distribution by an arbitrary angle does not change the energy of the system. Therefore, the ground state of the Wigner molecule is infinitely degenerate with respect to the orientation. Taking this degeneracy into account, one can construct the proper ground state of the Wigner molecule as the superposition of the rotated states associated with the particular space configuration. Recently, Yannoulenas and Landman [23] have reconstructed the cylindrically symmetric solutions using a post-treatment of the broken-symmetry HF solutions obtained with a multicentre basis similar to our basis (5). If, however, the rotational symmetry of the confining potential is slightly perturbed, the orientational degeneracy of the Wigner molecule is lifted and the Wigner molecule should be pinned under a fixed angle. The pinning of

the molecule under a fixed orientation is a necessary condition for direct observation of the Wigner molecule by wavefunction mapping [31]. In real QDs, the rotational symmetry of the confinement potential can be perturbed, e.g. because of the presence of impurities near the QD region or imperfections of the nanostructure.

In summary, we have performed a systematic study of phase transitions in Wigner molecules induced by an external magnetic field. We have proposed a multicentre Gaussian basis for the $N$-electron system and shown that this basis is sufficiently flexible to reproduce the properties of both the MDD and the molecular phases of the electron system. The results for the MDD do not depend upon the choice of the configuration of the Gaussian centres. We have determined the critical magnetic fields for the decay of the MDD into the molecular phase. The values of these fields are different for the different phases of the Wigner molecule created. We have found that the breakdown of the MDD is accompanied by a rapid jump of the electron–electron interaction energy as a function of the magnetic field. In the magnetic-field regime above the MDD breakdown, several molecular phases possess similar energies, but the phase with the lowest energy cannot in general be identified with the lowest-energy configuration of the classical point-charge system. We have shown that with increasing magnetic field the Wigner molecule, which consists of six or more electrons, undergoes several phase transitions. In particular, we have found new phases of the Wigner molecule which differ in their spatial distribution of electrons. For comparison, the Wigner crystal, which is created in the many-electron 2D system, possesses only one equilibrium phase with fixed (triangular) symmetry. On the contrary, based on the present results we predict that the few-electron Wigner molecules created in the QDs subjected to an external magnetic field are formed in several phases with a different symmetry. We have found that a search for the cusps in the expectation value of the electron–electron interaction energy as a function of the magnetic field can be proposed as a new condition, which is suitable when determining the Wigner molecule formation from the MDD phase. We have also suggested a solution to the controversy related to the possible mechanism of the MDD/Wigner molecule transition. Based on the results of the present paper, we suggest that for $N \leqslant 12$ the MDD decays from the centre, while for $N > 12$ edge reconstruction appears.

## Acknowledgment

This paper has been supported in part by the Polish Government Scientific Research Committee (KBN).

## References

[1] Wigner E P 1934 *Phys. Rev.* B **46** 1002
[2] Grimes C C and Adams G 1979 *Phys. Rev. Lett.* **42** 795
[3] Andrei E Y, Deville G, Williams F I B, Paris E and Etienne B 1988 *Phys. Rev. Lett.* **60** 2765
[4] Pudalov V M, D'Iorio M, Kravchenko S V and Campbell J W 1993 *Phys. Rev. Lett.* **70** 1866
[5] Jauregui K, Haüsler W and Kramer B 1993 *Europhys. Lett.* **24** 581
[6] Müller H M and Koonin S E 1996 *Phys. Rev.* B **54** 14532
[7] Maksym P A, Imamura H, Mallon G P and Aoki H 2000 *J. Phys.: Condens. Matter* **12** R299
[8] Reimann S M and Manninen M 2002 *Rev. Mod. Phys.* **74** 2002
[9] Yannouleas C and Landman U 1999 *Phys. Rev. Lett.* **82** 5325
[10] Szafran B, Bednarek S and Adamowski J 2002 *Phys. Rev.* B **65** 35361
[11] Reimann S M, Koskinen M, Manninen M and Mottelson B R 1999 *Phys. Rev. Lett.* **83** 3270
Reimann S M, Koskinen M and Manninen M 2000 *Phys. Rev.* B **62** 8108
[12] MacDonald A H, Yang E S R and Johnson M D 1993 *Aust. J. Phys.* **46** 345
[13] Yang E S R and MacDonald A H 2002 *Phys. Rev.* B **66** 041304

[14] Szafran B, Bednarek S and Adamowski J 2003 *Phys. Rev.* B **67** 045311 (erratum 159902(E))
[15] Szafran B, Bednarek S and Adamowski J 2003 *Phys. Rev.* B **67** 115323
[16] Bolton F and Rössler U 1993 *Supperlatt. Microstruct.* **13** 139
[17] Bedanov V M and Peeters F M 1994 *Phys. Rev.* B **49** 2667
[18] Schweigert V A and Peeters F M 1995 *Phys. Rev.* B **51** 7700
[19] Oosterkamp T H, Janssen J W, Kouwenhoven L P, Austing D G, Honda T and Tarucha S 1999 *Phys. Rev. Lett.* **82** 2931
[20] Price R, Zhu X, Das Sarma S and Platzman P M 1995 *Phys. Rev.* B **51** 2017
[21] Mikhailov S A 2001 *Physica* B **299** 6
[22] Kainz J, Mikhailov S A, Wensauer A and Rössler U 2002 *Phys. Rev.* B **65** 115305
[23] Yannoulenas C and Landman U 2002 *Phys. Rev.* B **66** 115315
[24] Bolton F 1994 *Solid-State Electron.* **37** 1159
[25] Dineykhan M and Nazmitdinov R G 1999 *J. Phys.: Condens. Matter* **11** L83
[26] Egger R, Häusler W, Mak C H and Grabert H 1999 *Phys. Rev. Lett.* **82** 3320
[27] Mikhailov S A 2002 *Physica* E **12** 884
[28] Reusch B, Häusler W and Grabert H 2001 *Phys. Rev.* B **63** 113313
[29] Manninen M, Viefers S, Koskinen M and Reimann S M 2001 *Phys. Rev.* B **64** 245322
[30] Chamon C de C and Wen X G 1994 *Phys. Rev.* B **49** 8227
[31] Vdovin E E, Levin A, Patanè A, Eaves L, Main P C, Khanin Yu N, Dubrovkii Yu V, Henini M and Hill G 2000 *Science* **290** 122

Eur. Phys. J. D **28**, 373–380 (2004)
DOI: 10.1140/epjd/e2003-00320-5

THE EUROPEAN PHYSICAL JOURNAL D

# Accuracy of the Hartree-Fock method for Wigner molecules at high magnetic fields

B. Szafran[1,2,a], S. Bednarek[1], J. Adamowski[1], M.B. Tavernier[2], E. Anisimovas[2], and F.M. Peeters[2]

[1] Faculty of Physics and Nuclear Techniques, AGH University of Science and Technology, Kraków, Poland
[2] Departement Natuurkunde, Universiteit Antwerpen (UIA), 2610 Antwerpen, Belgium

Received 18 August 2003 / Received in final form 24 October 2003
Published online 6 January 2004 – 

**Abstract.** Few-electron systems confined in two-dimensional parabolic quantum dots at high magnetic fields are studied by the Hartree-Fock (HF) and exact diagonalization methods. A generalized multicenter Gaussian basis is proposed in the HF method. A comparison of the HF and exact results allows us to discuss the relevance of the symmetry of the charge density distribution for the accuracy of the HF method. It is shown that the energy estimates obtained with the broken-symmetry HF wave functions become exact in the infinite magnetic-field limit. In this limit the charge density of the broken-symmetry solution can be identified with the classical charge distribution.

**PACS.** 73.20.Qt Electron solids – 73.21.-b Electron states and collective excitations in multilayers, quantum wells, mesoscopic, and nanoscale systems

## 1 Introduction

Properties of electron systems confined in quantum dots at high magnetic fields have recently become a subject of intensive theoretical studies [1–22]. These studies were inspired on the one hand by the experimental investigation of the addition spectra of vertical quantum dots [23] at high magnetic fields, which revealed a rich structure of magnetic-field induced ground-state transformations in the confined electron system [1–27], and on the other hand by the search for a new symmetry in few-electron systems. One of the most interesting problems in this research is the possibility of the formation of Wigner molecules [2–10,25–27] in which the confined electrons are distinctly spatially separated. Previous theoretical studies are based on the Hartree-Fock (HF) method [2–6,8], density functional theory (DFT) [9], and the exact diagonalization (ED) scheme [11–21]. The model confinement potential used most commonly [1–19] is the two-dimensional (2D) cylindrically symmetric harmonic oscillator potential, which is a reasonable approximation of the confinement potential [28] in vertical quantum dots [23].

The external magnetic field induces ground-state transformations in the quantum-dot confined $N$-electron system, which are associated with changes of the total angular momentum and the total spin. At a certain magnetic field the electrons become spin polarized and occupy the lowest-energy Fock-Darwin states with the $z$ component of the angular momentum changing from 0 to $(1-N)\hbar$ [10]. This state is called a maximum density droplet (MDD) [1]. In the MDD the $z$ components of the total spin and total angular momentum take on the absolute values $N\hbar/2$ and $N(N-1)\hbar/2$, respectively. The MDD ground state is predicted by the ED method [16–20] as well as by the HF [2] and DFT [9] methods. Higher magnetic fields lead to a decay of the MDD, which has been observed experimentally [23]. This decay, considered in the framework of the ED method [16,17], is related to the increase of the absolute value of the total angular momentum above the value corresponding to the MDD phase. The unrestricted HF [2–5] and DFT [9] methods predict that the ground state of the electron phase created after the decay of the MDD possesses a charge density which does not reproduce the symmetry of the external confinement potential. These states will be called "broken-symmetry states" throughout the present paper. In the broken-symmetry solutions obtained by the HF and DFT methods, the electrons become localized at separate space sites forming a Wigner molecule [2,5–7,9,10,25–27]. In the ED method the separation of the electrons, i.e., the formation of the Wigner molecules, appears in the relative coordinates of the electron system and is not necessarily related to the broken symmetry of the charge density [10]. The HF broken-symmetry solutions are not eigenfunctions of the angular momentum operator, but are degenerate with respect to rotations, i.e., can be oriented at an arbitrary angle. The rotational symmetry of the HF broken-symmetry solutions for the few-electron system can be restored with a post-HF treatment [4].

A multicenter basis with the one-electron wave functions was used in the theoretical studies of the 2D Wigner crystals [29,30]. Recently, a similar multicenter basis was

[a] e-mail: bszafran@agh.edu.pl

used [4–7] to study the quantum-dot confined electron systems. The papers [4–7] were based on the unrestricted HF method [4–6] and the variational method [7] with the trial wave function in the form of a single Slater determinant with non-orthogonal one-electron wave functions. These one-electron wave functions [4–7] at high magnetic field yield point-like charge density distributions. Therefore, in the limit of infinite magnetic field, the ground-state charge density, obtained with the multicenter basis, is identical with the lowest-energy classical configuration of the point charges [31–33]. The multicenter basis is a very efficient tool for the investigation of the Wigner molecules, since it requires only a single basis function per electron, while the convergence of the HF energy estimates in the one-center Fock-Darwin basis [2] is very slow in the regime of the island-like Wigner localization. Using the unrestricted HF method with the multicenter basis (MCHF), Szafran et al. [5] have shown that the external magnetic field leads to transformations of the ground-state symmetry of the Wigner molecules. Only in the high magnetic field limit the ground-state phase (isomer of the Wigner molecule) [5] corresponds to the configuration of electrons, which is identical with that of a classical system of point charges [31–33].

In the present paper, we perform a detailed study of the physics behind the formation of the Wigner molecules. In particular, we discuss the accuracy of the broken symmetry solutions obtained with the multicenter basis in comparison with the ED results for two, three, and four electrons. The physical interest of this study relies on the investigation of the quantum systems in a classical localization limit.

The paper is organized as follows: in Section 2 we briefly describe the theoretical methods, in Section 3 we present our numerical results, in Section 4 — the discussion, and in Section 5 — the conclusions and the summary. In Appendix, we derive the wave function used in the present calculations.

## 2 Theory

We consider the $N$-electron system confined in the 2D harmonic oscillator potential with frequency $\omega_0$, subject to the external magnetic field $B$ oriented perpendicularly to the quantum dot plane [5,6]. We apply the MCHF and ED methods. In the MCHF method we assume that all the electrons are spin polarized by the magnetic field and apply the Landau gauge, i.e., $\mathbf{A} = (-By, 0, 0)$. We expand one-electron wave function $\Psi_\mu(\mathbf{r})$ of the $\mu$th occupied state ($\mu = 1, ..., N$)

$$\Psi_\mu(\mathbf{r}) = \sum_{i=1}^{N} c_i^\mu \psi_{\mathbf{R}_i}(\mathbf{r}), \tag{1}$$

in the basis

$$\psi_{\mathbf{R}}(\mathbf{r}) = (\alpha/2\pi)^{1/2} \exp\{-(\alpha/4)\,(\mathbf{r}-\mathbf{R})^2 + (i\beta/2)(x-X)(y+Y)\}, \tag{2}$$

where $\mathbf{R} = (X, Y)$, $\mathbf{r} = (x, y)$, and $\alpha$ and $\beta$ are treated as nonlinear variational parameters. Function (2) with $\alpha = \beta = m^*\omega_c/\hbar$ is the wave function of the lowest Landau level ($\omega_c = eB/m^*$ is the cyclotron frequency and $m^*$ is the electron effective mass). Moreover, function (2) with $\alpha = (2m^*/\hbar)\sqrt{\omega_0^2 + \omega_c^2/4}$ and $\beta = m^*\omega_c/\hbar = eB/\hbar$ is the eigenfunction of the Fock-Darwin ground state for the lateral parabolic confinement potential centered at point $\mathbf{R}$ with the energy equal to $\hbar\sqrt{\omega_0^2 + \omega_c^2/4}$ (see Appendix). The probability density associated with wave function (2) is the Gaussian centered around point $\mathbf{R}$. The centers of basis functions (2) are taken from scaled configurations $\{\mathbf{R}^{class}\}$ of classical Wigner molecules, i.e., $\{\mathbf{R}\} \equiv \mathbf{R}_i = \sigma\mathbf{R}_i^{class}$, where $i = 1, ..., N$ [5,6]. The scaling parameter $\sigma$ is the third nonlinear variational parameter used in the present approach. In references [5,6] only two nonlinear variational parameters were used, namely, the scaling parameter $\sigma$ and a single variational parameter $\alpha = \beta$. In the following, we will show that the introduction of the two independent variational parameters in the real and imaginary part of the exponent in equation (2) leads to a significant improvement of the variational energy estimates at finite magnetic field. Throughout the present paper, the basis with the restriction $\alpha = \beta$ will be referred to as "restricted" and without it as "generalized".

In the present paper we also apply the ED method. The ED results, that in principle are the exact solutions of the few-electron Schrödinger equation, are used as reference data for the estimation of the accuracy of the MCHF results. In the ED calculations we use the symmetric gauge ($\mathbf{A} = (-By/2, Bx/2, 0)$), that allows us to exploit the angular symmetry of the one-electron wave functions. The Schrödinger equation for the $N$-electron system can be separated into the center-of-mass and relative-coordinate equations [15,19,22]. The center-of-mass eigenproblem possesses an analytical solution. For $N = 2$ the relative-motion eigenproblem can be easily solved numerically with an arbitrary precision using a one-dimensional finite difference method. This approach [15,19], used in the present paper for the two-electron system, is not applicable to the systems with a larger number of electrons. Thus, for $N = 3$ and $N = 4$ the ED procedure is constructed according to the configuration interaction method. First, we solve the Schrödinger equation for a single noninteracting electron with a definite angular momentum using a finite-difference approach on the one-dimensional mesh with 200 points. Next, we use the single-electron wave functions to construct Slater determinants with the required total angular momentum and spin. The $N$-electron Schrödinger equation is diagonalized in the orthonormal basis of Slater determinants with proper spin-orbital symmetry and the Coulomb matrix elements are integrated numerically. The basis, i.e., the choice of the single-electron wave functions forming the Slater determinants, is optimized separately for each state. The calculations have been performed with a precision better than 0.01 meV. For $N = 4$ this precision requires the application of the basis containing up to 2000 Slater determinants. The ED calculations of the ground state for $N = 3$ and 4 are carried out up to 20 T

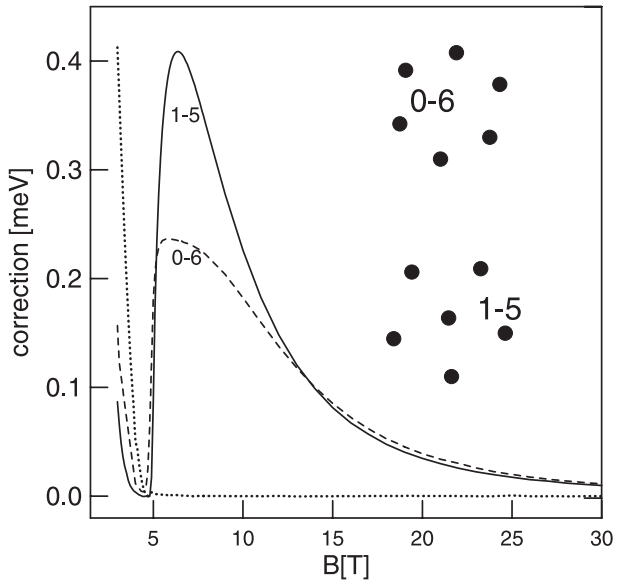


**Fig. 1.** Correction to the energy estimates obtained with the generalized MCHF method and calculated with respect to the results of the restricted HF method ($\alpha = \beta$) for the six-electron system with the configuration 1-5 (solid line) and 0-6 (dashed line) as a function of magnetic field $B$. The dotted line shows the overestimation of the energy obtained for 1-5 configuration with the value of $\beta$ fixed at $eB/\hbar$. Inset: the classical 0-6 and 1-5 Wigner molecules.

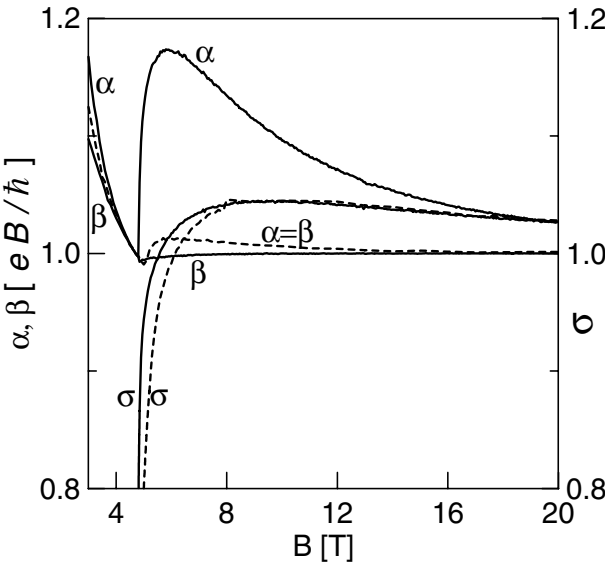


**Fig. 2.** Optimal values of the variational parameters for the 1-5 configuration obtained with the generalized ($\alpha \neq \beta$, solid lines) and restricted ($\alpha = \beta$, dashed lines) basis. Parameters $\alpha$ and $\beta$ are expressed in units $eB/\hbar$, parameter $\sigma$ is dimensionless.

with the maximal absolute values of the angular momentum equal to $18\hbar$ and $34\hbar$, respectively.

## 3 Results

Let us first discuss the corrections to the MCHF energy estimates obtained with the generalized wave function (2). We use as an example the system of six confined electrons. Figure 1 shows the difference between the energy estimates obtained with and without the restriction $\alpha = \beta$ in wave function (2). In the calculations we use the material parameters of GaAs, i.e. $m^* = 0.067m_e$, dielectric constant $\varepsilon = 12.9$, the effective Landè factor $g^* = -0.44$, and assume the confinement energy $\hbar\omega_0 = 3$ meV [2,5]. The centers of basis (1) are taken from scaled classical configurations 1-5 and 0-6 (the phases (isomers) of the Wigner molecule are labelled by the numbers of electrons localized in the subsequent rings starting from the innermost one). Phase 0-6 is the one, in which the Wigner molecule is created [5,10,14] after the MDD breakdown, and possesses an intermediate character. The 1-5 configuration is the lowest-energy configuration of the classical Wigner molecule [32]. This is also the ground-state configuration of the six-electron quantum system at high magnetic field [5]. In the magnetic field below 4.9 T the mutlicenter bases with both the 0-6 and 1-5 configurations mimic the cylindrically symmetric MDD charge distribution [5]. The correction obtained with the generalized basis possesses a minimum in the magnetic field inducing the MDD breakdown, for which, the application of the generalized basis does not improve the results. However, the generalized basis leads to considerable corrections to the energy both in the MDD stability regime and after the MDD breakdown. This correction falls down to zero in the high-magnetic field, in which both the generalized and restricted bases work with nearly the same precision.

The dotted line in Figure 1 shows the overestimation of the energy obtained for 1-5 configuration with fixed value of parameter $\beta = eB/\hbar$. The value of $\beta$ has an influence on the MCHF charge density due to the interference of the single-electron wave functions (Eqs. (1, 2)) centered at different sites. Figure 1 shows that the variation of $\beta$ has a large influence on the estimates of the energy in the MDD phase. On the other hand, in the Wigner molecule phase, the value of $\beta$ can be safely put equal to $eB/\hbar$.

Figure 2 shows the magnetic-field dependence of the optimal variational parameters obtained for the 1-5 configuration in expansion (1). The dependence of the scaling parameter $\sigma$ is qualitatively the same for both wave functions. This parameter grows rapidly when the MDD breaks down into the molecular phase. Generalized wave function (2) with $\alpha \neq \beta$ leads to the MDD decay at lower values of the magnetic field, which is visible in the dependence of $\sigma$ on the magnetic field. Parameter $\sigma$ tends to 1 at high magnetic fields for which the quantum Wigner molecule takes the shape and size of its classical analog, i.e., $\{\mathbf{R}\} \longrightarrow \{\mathbf{R}^{class}\}$. Parameters $\alpha$ and $\beta$ decrease with the increasing magnetic field in the MDD regime (cf. solid lines for $B \lesssim 5$ T in Fig. 2). Just before the MDD breakdown $\alpha$ and $\beta$ take on very close values, which leads to the minimal overestimation of the energy obtained with restriction $\alpha = \beta$ at the MDD breakdown (cf. Fig. 1). We have found that the increase of $\beta$ above $eB/\hbar$ in the MDD regime makes the local maxima of the charge density 'sink' in the global flat maximum characteristic [6]

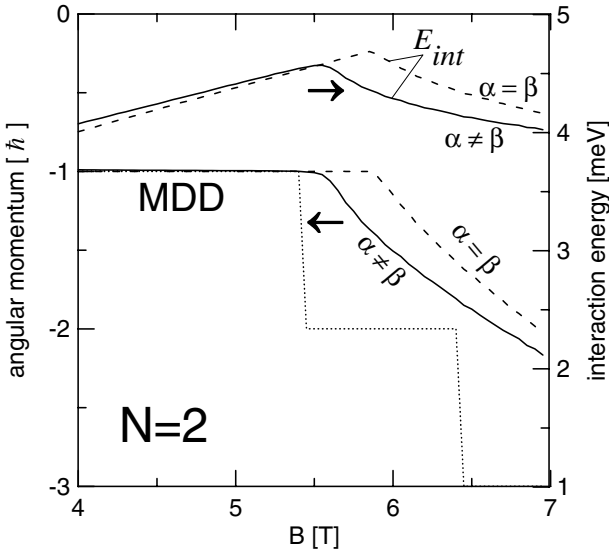


**Fig. 3.** Total angular momentum (left scale) of the exact ground state of the two-electron system (dotted line) and MCHF expectation values calculated with the generalized ($\alpha \neq \beta$, solid line) and the restricted ($\alpha = \beta$, dashed line) basis. The two curves marked by $E_{int}$ show the expectation value of the electron-electron interaction energy (right scale) calculated with the MCHF methods.

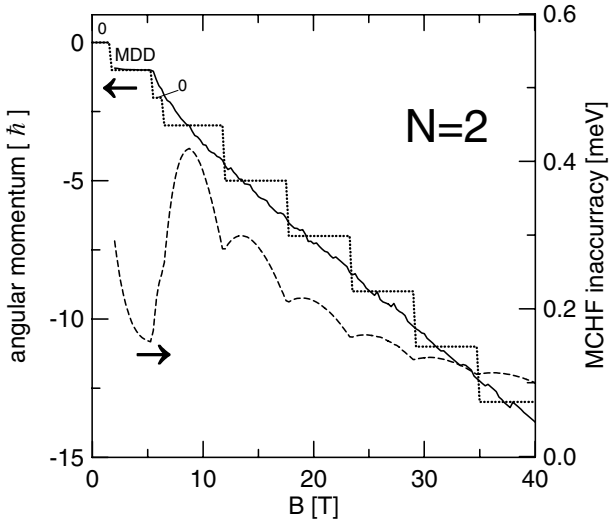


**Fig. 4.** Total angular momentum (left scale) of the exact ground state of the two-electron system (dotted line) and the MCHF expectation value calculated with the generalized basis (solid line) as functions of magnetic field $B$. The states with unpolarized spins are marked by "0". The dashed line shows the difference of the ground-state energy obtained with the MCHF and the exact energy calculated with the ED scheme (right scale).

for the MDD phase. After the MDD breakdown parameter $\beta$ quickly reaches $eB/\hbar$, i.e. takes on the value which corresponds to both the lowest Landau and Fock-Darwin levels (cf. the discussion of wave function (2) in Sect. 2). At high magnetic fields the wave functions (2) centered around different sites stop to overlap; in consequence, $\beta$ stops to influence the MCHF charge density and takes the value $eB/\hbar$, which ensures the equivalence of the centers of Landau orbitals. The present finding that the parameter $\beta$ becomes equal to $eB/\hbar$ just after the MDD breakdown, in spite of the non-vanishing overlap is not evident a priori. We can give the following physical interpretation to this finding: the electrons in the Wigner molecule behave as if they occupied the independent one-particle Fock-Darwin ground-state orbitals, each of them centered around its own local minimum of the potential energy. The optimal value of $\alpha$ rapidly grows after the MDD breakdown (cf. Fig. 2), which leads to the lowering of the energy obtained in the Wigner molecule regime ($B > 5$ T). The increase of $\alpha$ above $eB/\hbar$ enhances the electron localization and lowers the electron-electron interaction energy.

Figure 3 illustrates the MDD decay picture obtained with the ED and MCHF methods for the two-electron system. The dotted line shows the exact values of the $z$-component of the total angular momentum as a function of the magnetic field. The decay of the MDD is related with a stepwise decrease of the angular momentum from $-\hbar$ to $-2\hbar$, which appears for $B = 5.45$ T. The solid (dashed) line shows the expectation value of the total angular momentum obtained with the MCHF method using the generalized (restricted) basis. Figure 3 shows that within the MDD stability regime both the present MCHF methods reproduce the exact value of the angular momentum. When the MDD breaks down, the MCHF expectation value of the angular momentum decreases monotonically with the increasing $B$, in contrast to the exact stepwise behavior. The MDD breakdown obtained by the HF method is also related to a cusp of the interaction energy [6] (cf. two upper curves in Fig. 3). In the MDD regime the charge density distribution shrinks with increasing magnetic field, which results in an increase of the interaction energy. The transformation of the charge density from the droplet into the molecular phase occurs when the interaction energy exceeds some threshold value. The MCHF method with the generalized (restricted) basis leads to a MDD breakdown for $B = 5.55$ T (5.85 T).

Figure 4 displays the exact ground-state angular momentum for the two-electron system (dotted line) and the expectation value obtained within the HF method with the generalized multicenter basis (solid line) as well as the difference between the MCHF and the exact energy (dashed line). The $z$-component of the total spin is equal to $\hbar$ with the exception of the low-magnetic field ground state and the state which appears just after the MDD breakdown. These two states possess zero spin and are labelled by "0" in Figure 4. Notice that the expectation value of the total angular momentum follows quite well the exact value. Moreover, the overestimation of the ground state energy within the MCHF method decreases with increasing magnetic field. This decrease is non-monotonous, and the MCHF inaccuracy exhibit local minima for magnetic fields for which the exact angular momentum changes.

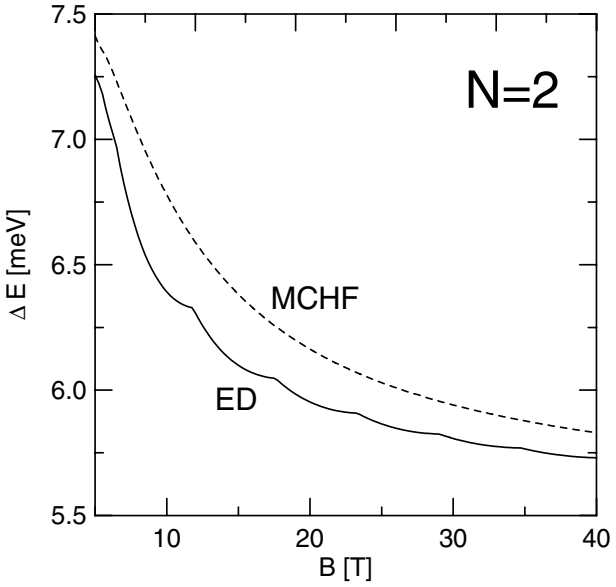


**Fig. 5.** Energy $\Delta E$ of the two-electron system calculated with respect to the lowest Landau level as a function of magnetic field $B$. Solid (dashed) curve show the exact (MCHF) results.

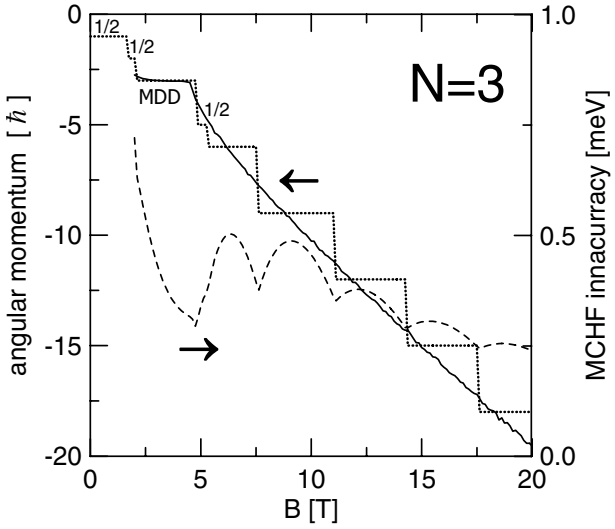


**Fig. 6.** Same as Figure 4 but now for the three-electron system. The states with unpolarized spins are marked with "1/2".

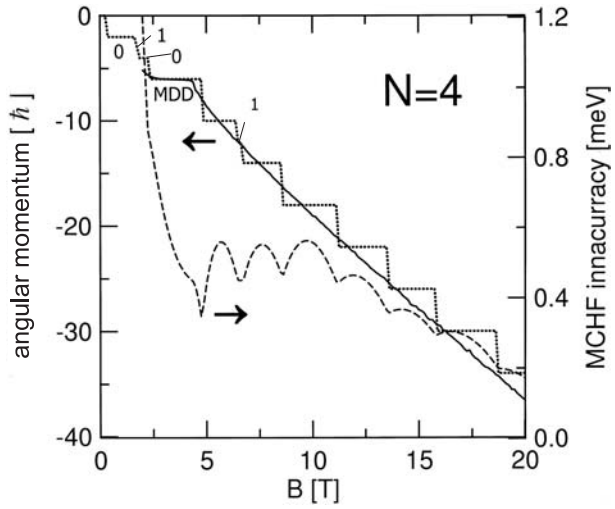


**Fig. 7.** Same as Figure 4 but now for the four-electron system. The states with unpolarized spins are marked with the value of the $z$-component of the total spin in $\hbar$ units.

The origin of this oscillatory behavior is explained in Figure 5, which shows the MCHF energy estimate and the exact ground-state energy of the two-electron system calculated with respect to the lowest Landau level, i.e., $\Delta E = E - 2(\hbar\omega_c/2 + \hbar g^* \mu_B B/2)$. The MCHF estimate is a smooth function of the magnetic field, while the exact energy possesses cusps at the magnetic fields at which the ground-state angular momentum changes abruptly. For these magnetic fields the MCHF estimate is visibly closer to the exact energy value, which explains the local minima in Figure 4.

A similar comparative study between the exact and the MCHF results has been made for the $N = 3$ and $N = 4$ systems. For the system of three electrons the results are shown in Figure 6, in which the ground states with the total spin equal to $\hbar/2$ are labelled by "1/2". The other states are fully spin polarized. Similarly as in the case of the two-electron system the ground state which appears after the MDD breakdown is not spin polarized. The overestimation of the total energy obtained with the MCHF method exhibits a similar qualitative dependence on the magnetic field as for two electrons. In contrast to the two-electron case, the MCHF method with the generalized basis predicts a breakdown of the MDD for a slightly smaller magnetic field value ($B = 4.6$ T) than the exact result ($B = 4.8$ T). The MCHF with the restricted basis yields the magnetic field inducing the MDD breakdown $B = 5$ T.

A similar result for the four-electron quantum dot is shown in Figure 7. The non-fully-polarized ground states are marked by the quantum numbers of the total-spin $z$-component "0" and "1". Contrary to the two and three electron systems, the four-electron MDD decays into a spin-polarized state, but a low-spin state still appears at the higher magnetic field. The transitional appearance of low-spin ground states at magnetic fields above the MDD breakdown have been reported first in reference [11] for $N = 2$ and $N = 4$. The exact magnetic field inducing the MDD decay is equal to 4.75 T, while the MCHF with the generalized basis predicts a value of 4.38 T and the MCHF with the restricted basis gives 4.8 T. In this case the MCHF with the restricted basis gives accidentally a better estimate for the MDD breakdown field. For five electrons the difference between both the MCHF estimates of the magnetic field inducing the MDD decay is 0.4 T. For six and more electrons the differences are not larger than 0.2 T.

Figures 4, 6, and 7 show that the MCHF inaccuracy decreases with the increasing magnetic field. In order to find the high-field asymptotic behavior of the MCHF energy estimate we have plotted in Figure 8 the MCHF error as a function of $1/B$ for $N = 2$, 3, and 4. The plot for two

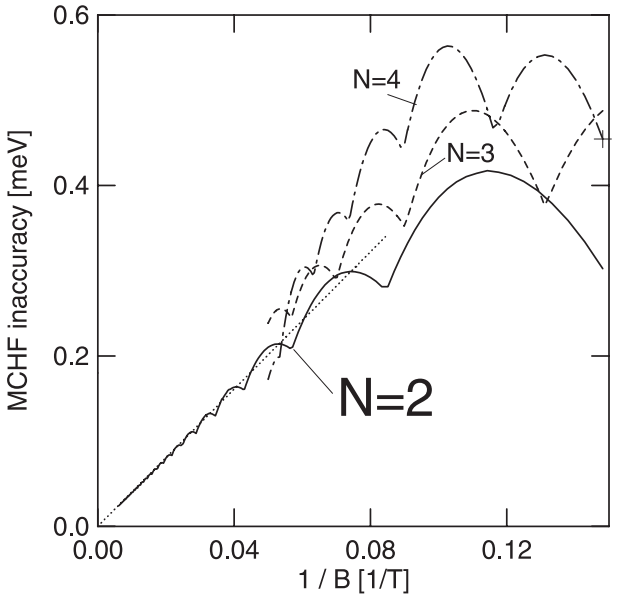


**Fig. 8.** The MCHF inaccuracy for the ground state for the two-electron system as a function of $1/B$ for $N = 2$ (solid line), 3 (dashed line) and 4 (dash-dotted line). The dotted line shows the high-magnetic field asymptote for $N = 2$, parametrized as $4.026/B$ (meV/T).

electrons covers the magnetic fields up to 160 T, while the plots for three and four electrons are drawn up to 20 T only. The results for $N = 2$ show that at high magnetic fields the MCHF inaccuracy is proportional to $1/B$. At high magnetic fields the asymptotic behavior of the MCHF inaccuracy for $N = 2$ can be very well approximated by the function $f(B) = 4.026/B$ (meV/T), and consequently the MCHF approach becomes exact for $B \to \infty$. The plots for $N = 3$ and 4 in the studied (narrower) range of the magnetic field exhibit a similar tendency as that for $N = 2$, however, they do not become linear functions of $1/B$ for $B < 20$ T. The comparison of the MCHF inaccuracies for $N = 2, 3$, and 4 indicates that the overestimation of the MCHF ground-state energy in the magnetic field range above the MDD instability does not substantially increase with $N$. For $B = 20$ T the overestimation of the ground-state energy for $N = 2, 3$, and 4 is equal to 0.21, 0.24, and 0.18 meV, respectively.

## 4 Discussion

Figures 4, 6 and 7 show that at high magnetic field the exact ground-state angular momentum take the so-called magic values [25,34–36] and change by $N\hbar$. Only for these magic values of the angular momenta the classical symmetry can be reproduced in the inner coordinates of the quantum systems [25]. On the other hand the classical symmetry is ensured in the MCHF by the present choice of centers of orbitals (2) and the linear change of the expectation value of the total angular momentum is related with the growing localization of wave functions (2).

The results presented in Figures 4, 6, 7, and 8 show that the broken-symmetry solutions obtained with the MCHF method provide exact energy results in the high magnetic field limit. This fact might be rather surprising, since one could expect that the exact solutions of the few-electron Schrödinger equation should also be the eigenfunctions of the angular momentum operator. The exact eigenfunctions yield the charge density distribution, which reproduces the symmetry of the confinement potential. This apparent contradiction can be solved if we consider the Schrödinger equation for the electron system confined in the parabolic potential. This equation can be separated in the center-of-mass and relative coordinates. In the framework of the ED approach, the separation of the electrons, i.e., the Wigner localization, appears in the relative (inner) coordinates of the electron system, while the charge density in the laboratory frame is affected by the center-of-mass motion. The center-of-mass eigenproblem of the few-electron system has the same form as the Fock-Darwin equation for the single electron. In the high magnetic field limit, this equation possesses a degenerate ground state (the lowest Landau state), for which the angular momentum is arbitrary. In the case of this degeneracy a superposition of ground states with different angular momenta is still the ground state of the Fock-Darwin equation, even though it leads to solutions with the broken symmetry of the charge density distribution in the laboratory frame. In the HF method, the formation of the Wigner molecule, i.e., the separation of the electrons, is only possible in the broken-symmetry solutions. The results of the present paper show that exact energy is obtained with these broken-symmetry solutions in the infinite magnetic field limit.

In the recent paper of Bednarek et al. [37] a study of the accuracy of the HF method has been presented for the quasi-one-dimensional (1D) structure. In the quasi-1D structures the unrestricted HF method becomes exact [37] in the large quantum dots, in which the Wigner molecules are formed [37]. In the 1D structures, the HF method conserves the two-particle parity symmetry of the exact solution; so, there is no problem with the broken symmetry of the HF solutions like in the 2D circularly symmetric quantum dots.

The present results show that the overestimation of the exact energy obtained in the broken-symmetry MCHF solutions is relatively small at the magnetic fields, for which the ground state is degenerate. The ground state of the few-electron system is twofold degenerate at these magnetic fields, which induce a stepwise change of the ground-state angular momentum (cf. Figs. 4, 6, and 7). In this case, the exact ground state can be a superposition of two states with different angular momenta and therefore the charge density can have the symmetry different from that of the external potential. For these fields the broken symmetry of the HF solutions leads to the decrease of the energy separation between the MCHF and ED results (cf. Fig. 6), which in turn causes the characteristic oscillations of the MCHF error as a function of the magnetic field as shown in Figures 4–7.

The application of the generalized variational basis results in a modification of the phase diagram [5], for the Wigner molecules. This modification is due to the different precision of the restricted wave function for different phases (cf. Fig. 1). The critical magnetic fields for the MDD breakdown, obtained with the generalized basis, are shifted toward lower values (cf. Fig. 3) and the range of the stability of different phases is modified. The improved results conserve the characteristic features of the original phase diagram [5] i.e., the intermediate phases correspond to the configurations, for which a larger number of electrons is gathered on the outer ring of the molecule in comparison with the classical, high-magnetic-field, ground-state configuration.

The present calculations performed for small number of electrons indicate that in the high magnetic field the inner charge distribution of electrons can be derived from classical calculations for particles interacting via a Coulomb $(1/r)$ interaction. On the other hand in the Laughlin wave function [38], which seems to be an exact description of the many-body state at high magnetic field, the distribution of electrons in the inner coordinates corresponds to classical configuration of particles interacting with a logarithmic potential. It is therefore not excluded that for larger number of electrons the localization may be different than for electrostatically interacting classical particles.

## 5 Conclusions and summary

We have investigated the quantum-dot confined $N$-electron system at high magnetic fields using the HF method with the generalized multicenter basis and the exact diagonalization method. We have indicated that the magnetic-field dependence of the variational parameters of the generalized basis can be used as one of the signatures of the liquid-solid phase transition, i.e., the breakdown of the MDD into the molecular phase. The occurrence of the cusp of the interaction energy as a function of the magnetic field and the decrease of the MCHF angular-momentum expectation value below that corresponding to the MDD are the other signatures of the MDD decay. We have discussed the accuracy of the energy estimates obtained with the broken-symmetry HF solutions, which — in contrast to the exact solutions of the Schrödigner equation — are not eigenfunctions of the total angular-momentum operator. It turns out that the angular-momentum eigenvalues in the MDD phase are reproduced with the high accuracy by the MCHF expectation values, which at higher magnetic fields linearly decrease with increasing $B$ in contrast to the exact stepwise decrease. The results of the present paper show that the MCHF inaccuracy decreases with the increasing magnetic field and that the MCHF method basis yields the exact ground-state energy in the infinite magnetic-field limit. We have found the characteristic oscillations of the HF inaccuracy, which exhibits local minima at those magnetic fields, for which the exact ground state is degenerate with respect to the angular momentum. The relation of these oscillations with the existence of the exact ground states with the broken symmetry has been pointed out. The results of the present paper show that the envelope of the MCHF inaccuracy oscillations at high magnetic field decreases linearly to 0 as a function of $1/B$ and that in the strictly infinite magnetic field limit the exact energy is obtained for the broken-symmetry HF solution with the classical point-charge distribution.

This work was supported in part by the Polish Government Scientific Research Committee (KBN), the Flemish Science Foundation (FWO-Vl), IUAP, and GOA. One of us (EA) is supported by a EU Marie Curie fellowship. The first author (BS) is supported by the Foundation for Polish Science (FNP).

## Appendix

In order to derive wave function (Eq. (2)) let us first consider the single electron in a homogeneous magnetic field. In the Landau gauge, i.e., for $\mathbf{A}(\mathbf{r}) = (-By, 0, 0)$, the Hamiltonian has the form

$$H_0 = -\frac{\hbar^2}{2m^*}\left(\frac{\partial^2}{\partial x^2} + \frac{\partial^2}{\partial y^2}\right) + i\hbar\omega_c y\frac{\partial}{\partial x} + \frac{m^*\omega_c^2}{2}y^2, \quad (3)$$

where $\omega_c = eB/m^*$. The lowest Landau energy level $E_0 = \hbar\omega_c/2$ is infinitely-fold degenerate. The corresponding degenerate eigenstates have the form

$$\chi_q(x,y) = C_1 \exp\left[iqx - (\beta/2)(y - q/\beta)^2\right], \quad (4)$$

where $\beta = m^*\omega_c/\hbar = eB/\hbar$, $C_1$ is the normalization constant, and $q \in (-\infty, +\infty)$. Due to this degeneracy, an arbitrary linear combination of wave functions (4) is an eigenfunction of Hamiltonian (3) to eigenvalue $E_0$. The most general form of this linear combination can be written as

$$\psi_0(x,y) = \int_{-\infty}^{+\infty} f(q)\chi_q(x,y)\,dq. \quad (5)$$

Taking

$$f(q) = \exp\left[q(y_0 - ix_0) - q^2/2\beta\right] \quad (6)$$

and performing the integration in equation (5), we obtain

$$\psi_0(x,y) = C_0 \exp\{-(\beta/4)\left[(x-x_0)^2 + (y-y_0)^2\right] + (i\beta/2)(x-x_0)(y+y_0)\}, \quad (7)$$

where $C_0$ is the normalization constant. Wave function (7) corresponds to the electron probability density, which is localized around center $\mathbf{r}_0 = (x_0, y_0)$. For arbitrary $\mathbf{r}_0$ wave function (7) is the eigenfunction of the Hamiltonian (3) associated with eigenvalue $E_0$. Due to the arbitrary choice of $\mathbf{r}_0$, wave functions (7), localized at different centers, correspond to the same lowest Landau level.

If, in addition to the magnetic field, the electron is subject to the external parabolic potential centered at site $\mathbf{R} = (X, Y)$, i.e.,

$$V_{conf}(x,y) = \frac{m^*\omega_0^2}{2}[(x-X)^2 + (y-Y)^2], \quad (8)$$

we deal with the Fock-Darwin eigenproblem. Then, the ground-state wave function is centered around $\mathbf{R}$ and is written down in the normalized form as

$$\psi_{(X,Y)}(x,y) = \exp\{-(\alpha/4)\left[(x-X)^2+(y-Y)^2\right] + (i\beta/2)(x-X)(y+Y)\}/(\alpha/2\pi)^{1/2}, \quad (9)$$

where $\alpha = (2m^*/\hbar)\sqrt{\omega_0^2+\omega_c^2/4}$. Therefore, we obtain the wave function of form (2).

## References


1. A.H. MacDonald, S.R.E. Yang, M.D. Johnson, Aust. J. Phys. **46**, 345 (1993)
2. H.-M. Müller, S.E. Koonin, Phys. Rev. B **54**, 14532 (1996)
3. C. Yannouleas, U. Landman, Phys. Rev. B **61**, 15895 (2000)
4. C. Yannouleas, U. Landman, Phys. Rev. B **66**, 115315 (2002)
5. B. Szafran, S. Bednarek, J. Adamowski, Phys. Rev. B **67**, 045311 (2003); *erratum*, Phys. Rev. B **67**, 159902(E) (2003)
6. B. Szafran, S. Bednarek, J. Adamowski, J. Phys. Condens. Matt. **15**, 4189 (2003)
7. J. Kainz, S.A. Mikhailov, A. Wensauer, U. Rössler, Phys. Rev. B **65**, 115305 (2002)
8. B. Reusch, H. Grabert, Phys. Rev. B **68**, 045309 (2003)
9. S.M. Reimann, M. Koskinen, M. Manninen, B.R. Mottelson, Phys. Rev. Lett. **83**, 3270 (1999)
10. S.M. Reimann, M. Manninen, Rev. Mod. Phys. **74**, 1283 (2002)
11. P.A. Maksym, T. Chakraborty, Phys. Rev. B **45**, 1947 (1992)
12. M. Eto, Jpn J. Appl. Phys. **36**, 3924 (1997)
13. H. Immamura, P.A. Maksym, H. Aoki, Physica B **249-251**, 214 (1998)
14. M. Manninen, S. Viefers, M. Koskinen, S.M. Reimann, Phys. Rev. B **64**, 245322 (2001)
15. A. Matulis, F.M. Peeters, Solid State Comm. **117**, 655 (2001)
16. S.A. Mikhailov, N.A. Savostianova, Phys. Rev. B **66**, 033307 (2002)
17. S.R.E. Yang, A.H. MacDonald, Phys. Rev. B **66**, 041304 (2002)
18. A. Wójs, P. Hawrylak, Phys. Rev. B **56**, 13227 (1997)
19. M. Dineykhan, R.G. Nazmitdinov, J. Phys. Condens. Matt. **11**, L83 (1999)
20. B. Szafran, S. Bednarek, J. Adamowski, Phys. Rev. B **67**, 115323 (2003)
21. M. Rontani, G. Goldoni, F. Manghi, E. Molinari, Europhys. Lett. **58**, 555 (2002)
22. F.M. Peeters, Phys. Rev. B **42**, 1486 (1990)
23. T.H. Oosterkamp, J.W. Janssen, L.P. Kouwenhoven, D.G. Austing, T. Honda, S. Tarucha, Phys. Rev. Lett. **82**, 2931 (1999)
24. B. Szafran, S. Bednarek, J. Adamowski, Phys. Rev. B **65**, 035316 (2002)
25. P.A. Maksym, H. Immamura, G.P. Mallon, H. Aoki, J. Phys. Condens. Matt. **12**, R299 (2000)
26. R. Egger, W. Häusler, C.H. Mak, H. Grabert, Phys. Rev. Lett. **82**, 3320 (1999)
27. S. Akbar, I.-H. Lee, Phys. Rev. B **63**, 165301 (2001)
28. S. Bednarek, B. Szafran, J. Adamowski, Phys. Rev. B **64**, 195303 (2001)
29. K. Maki, X. Zotos, Phys. Rev. B **28**, 4349 (1983)
30. R. Price, X. Zhu, S. Das Darma, P.M. Platzmann, Phys. Rev. B **51**, 2017 (1999)
31. F. Bolton, U. Rössler, Superlatt. Microstruct. **13**, 139 (1993)
32. V.M. Bedanov, F.M. Peeters, Phys. Rev. B **49**, 2667 (1994)
33. M. Kong, B. Partoens, F.M. Peeters, Phys. Rev. E **65**, 046602 (2002)
34. S.M. Girvin, T. Jach, Phys. Rev. B **28**, 4506 (1983)
35. P.A. Maksym, Phys. Rev. B **53**, 10871 (1996)
36. C.G. Bao, W.Y. Ruan, Y.Y. Liu, Phys. Rev. B **53**, 10820 (1996)
37. S. Bednarek, T. Chwiej, J. Adamowski, B. Szafran, Phys. Rev. B **67**, 205316 (2003)
38. R.B. Laughlin, Phys. Rev. B **27**, 3383 (1983)